Plasma Physics and
Controlled Fusion

PURPOSE-LED
PUBLISHING™

PAPER • **OPEN ACCESS**

Overview of the third JET deuterium-tritium campaign

To cite this article: A Kappatou *et al* 2025 *Plasma Phys. Control. Fusion* **67** 045039

View the article online for updates and enhancements.

You may also like

- Comparison of deconvolution techniques for 1D neutron emission profile reconstruction using ITER Radial Neutron Camera synthetic data and JET neutron camera measurements
Katarzyna Mikszuta-Michalik, Daniele Marocco, Basilio Esposito et al.
- First observations of edge instabilities in strongly shaped negative triangularity plasmas on DIII-D
T Cote, G Yu, A O Nelson et al.
- Tungsten control in long pulse operation: feedback from WEST to ITER
P Maget, P Manas, J Morales et al.

This content was downloaded from IP address 134.94.123.71 on 05/03/2026 at 10:07

OPEN ACCESS
IOP Publishing
Plasma Physics and Controlled Fusion
Plasma Phys. Control. Fusion **67** (2025) 045039 (19pp)
https://doi.org/10.1088/1361-6587/adbd75

Overview of the third JET deuterium-tritium campaign

A Kappatou[1,*], M Baruzzo[2], A Hakola[3], E Joffrin[4], D Keeling[5], B Labit[6], E Tsitrone[4], N Vianello[7], M Wischmeier[1], I Balboa[5], J Bernardo[5], M Bernert[1], T Bosman[8,9], S Brezinsek[10], D Brida[1], I S Carvalho[11], P Carvalho[5], L Ceelen[8,9], C D Challis[5], I Coffey[5], T Dittmar[10], M Dunne[1], M Faitsch[1], A R Field[5], L Frassinetti[12], L Garzotti[5], Z Ghani[5], C Giroud[5], S Henderson[5], R B Henriques[5], J Hobirk[1], P Jacquet[5], I Jepu[5], Ye O Kazakov[13], D B King[5], K K Kirov[5], D Kos[5], K Krieger[1], M Lennholm[5], E Lerche[13], X Litaudon[4], E Litherland-Smith[5], P Lomas[5], C Lowry[5], J Mailloux[5], M J Mantsinen[14], M Maslov[5], D Matveev[10], A Meigs[5], S Menmuir[5], C Olde[5], C Perez von Thun[15], L Piron[7], G Pucella[2], H Reimerdes[6], F Rimini[5], O Sauter[6], P A Schneider[1], B Sieglin[1], S Silburn[5], E R Solano[16], H Sun[5], D F Valcarcel[5], D van Eester[13], R Villari[2], A Widdowson[5], S Wiesen[8], M Zlobinski[10], V K Zotta[17], the JET contributors[18] and the EUROfusion Tokamak Exploitation Team[19]

[1] Max-Planck-Institut für Plasmaphysik, Boltzmannstr. 2, 85748 Garching, Germany
[2] Nuclear Department, ENEA, Frascati, Italy
[3] VTT Technical Research Centre of Finland Ltd, Espoo, Finland
[4] CEA, IRFM, Saint-Paul-lez-Durance, France
[5] United Kingdom Atomic Energy Authority, Culham Campus, Abingdon, Oxfordshire OX14 3DB, United Kingdom
[6] École Polytechnique Fédérale de Lausanne (EPFL), Swiss Plasma Center (SPC), CH-1015 Lausanne, Switzerland
[7] Consorzio Consorzio RFX, ISTP, Padova, Italy
[8] DIFFER-Dutch Institute for Fundamental Energy Research, Eindhoven, The Netherlands
[9] Dept. of Mechanical Engineering, Control Systems Technology Group, Eindhoven University of Technology, Eindhoven, The Netherlands
[10] Forschungszentrum Jülich GmbH, Institute of Fusion Energy and Nuclear Waste Management—Plasma Physics, 52425 Jülich, Germany
[11] ITER Organization, Route de Vinon-sur-Verdon, CS 90 046, 13067 St Paul Lez Durance Cedex, France
[12] KTH Royal Institute of Technology, Stockholm, Sweden
[13] Laboratory for Plasma Physics, LPP-ERM/KMS, Brussels B-1000, Belgium
[14] ICREA and Barcelona Supercomputing Center, Barcelona, Spain
[15] Institute of Plasma Physics and Laser Microfusion, Hery 23, 01-497 Warsaw, Poland
[16] Laboratorio Nacional de Fusión, CIEMAT, Madrid, Spain
[17] Dipartimento di Ingegneria Astronautica, Elettrica ed Energetica, Sapienza Universitá di Roma, via Eudossiana 18, 00184 Roma, Italy

E-mail: athina.kappatou@ipp.mpg.de

Received 31 October 2024, revised 28 February 2025
Accepted for publication 6 March 2025
Published 10 April 2025

[18] See Maggi *et al* 2024 (https://doi.org/10.1088/1741-4326/ad3e16) for the JET contributors.
[19] See Joffrin *et al* 2024 (https://doi.org/10.1088/1741-4326/ad2be4) for the EUROfusion Tokamak Exploitation Team.
[*] Author to whom any correspondence should be addressed.

Original Content from this work may be used under the terms of the Creative Commons Attribution 4.0 licence. Any further distribution of this work must maintain attribution to the author(s) and the title of the work, journal citation and DOI.

© 2025 The Author(s). Published by IOP Publishing Ltd

Abstract

JET returned to deuterium-tritium operations in 2023 (DTE3 campaign), approximately two years after DTE2. DTE3 was designed as an extension of JET's 2022-2023 deuterium campaigns, which focused on developing scenarios for ITER and DEMO, integrating in-depth physics understanding and control schemes. These scenarios were evaluated with mixed D-T fuel, using the only remaining tritium-capable tokamak until its closure in 2023. A core-edge-SOL integrated H-mode scenario was developed and tested in D-T, showing good confinement and partial divertor detachment with Ne-seeding. Stationary pulses with good performance, no tungsten accumulation, and even without ELMs were achieved in D-T. Plasmas with pedestals limited by peeling modes were studied with D, T-rich, and D-T fuel, revealing a positive correlation between pedestal electron pressure and pedestal electron density. The Quasi-Continuous Exhaust regime was successfully achieved with D-T fuel, with access criteria similar to those in D plasmas. A scenario with full detachment, the X-point radiator regime, was established in D-T, aided by the real-time control of the radiator's position. The crucial characterisation of tritium retention continued in DTE3, using gas balance measurements and the new LID-QMS diagnostic. Nuclear technology studies were advanced during the DTE3 campaign, addressing issues such as the activation of water in cooling loops and single event effects on electronics. Building on the previous D, T and DTE2 campaigns and the lessons learned from them, DTE3 extended our understanding of D-T plasmas, particularly in scenarios relevant to next-generation devices such as ITER and DEMO.

Keywords: Deuterium-tritium, D-T, JET, isotope, fusion energy, tritium

1. Introduction

Future fusion reactors will operate with a mixed fuel of deuterium and tritium. Nowadays almost all devices operate with hydrogen and deuterium. JET has been a notable exception due to its ability to operate with tritium. Experiments with a deuterium and tritium fuel mix are crucial for the preparation towards next step devices, such as ITER or a demonstration fusion power plant. From the plasma physics point of view, understanding how the change in the isotope mass affects the plasma confinement and transport from the core to the edge of the plasma and the plasma-wall interaction processes is crucial. Furthermore, the fusion-born α-particles are expected to transfer their energy to the plasma via collisions and provide the self-heating required to achieve a 'burning' plasma. From the technical point of view, experience in operations in a nuclear environment is required. This involves understanding the irradiation of materials, the impact on diagnostics, as well as waste management. Finally, information on the tritium cycle and fuel retention, key to define and inform regulatory and safety aspects is necessary. As such, deuterium-tritium experiments are indispensable for the preparation towards next step devices.

Only two magnetic confinement fusion devices have ever had the capability to handle tritium; JET was until its shutdown at the end of 2023 [1], the only device capable of handling tritium, after the shutdown of TFTR in 1997 [2–4]. Furthermore, JET is capable of confining α-particles (for a plasma current typically above 2.5MA) [5]. After the Preliminary Tritium Experiments (PTE) in 1991 [6], JET executed its first deuterium-tritium campaign with a substantial concentration of tritium (DTE1) in 1997 [7, 8]. This was followed by the Trace Tritium experiments (TTE) in 2003. Following the change of the plasma facing components from carbon to all metal plasma facing components (beryllium main chamber and tungsten divertor) [9], JET returned to deuterium-tritium operations in 2021 (DTE2 campaign [10]) and again in 2023 (DTE3 campaign).

For the last two years of its operation (2022–2023), JET was incorporated in the EUROfusion Consortium Work Package Tokamak Exploitation (WPTE), along with the other major European tokamaks (namely, ASDEX Upgrade, MAST Upgrade, TCV and WEST). In its conception, the WPTE scientific program is realising the EUROfusion programme, based on the European Research Roadmap to the Realisation of Fusion Energy [11], and is aiming to address key questions for ITER and DEMO[20], developing plasma regimes of operation and heat exhaust solutions, by integrating the physics understanding with control tools [12]. The experimental program and its scientific priorities were defined across the devices, strengthening the link and knowledge transfer between the medium-size tokamaks and JET. Most importantly, it encourages even further the efforts to transfer scenarios developed in smaller devices to JET, to investigate the machine size impact on the scenarios and to expand the parameter space in which these scenarios exist.

This article provides an overview of the third and last deuterium-tritium campaign at JET in 2023 (DTE3). The design and scientific objectives of these experiments are described in section 2, and the experiments addressing each

[20] Herein, DEMO refers to the European DEMO envisioned in the 'European Research Roadmap to the Realisation of Fusion Energy', though many of the key questions will be applicable to any future demonstration fusion power plant.

of these objectives are detailed in sections 3–10, with a summary and discussion in section 11. As the detailed analysis and modelling of the experimental data is underway, the aim of this article is to provide an overview of the experiments and share the first observations. Future publications will discuss in more detail the in-depth physics understanding and more importantly, the predictions that can be made for future devices.

2. The DTE3 campaign design and objectives

The tritium and deuterium-tritium (DTE2) campaigns in 2021–2022 were designed on a set of explicit goals [10]. A major part of the deuterium campaigns preceding these were dedicated to the preparation of the scenarios and pulses for D-T operations [5, 13], with emphasis on the demonstration of the integration of sustained high fusion power production with the Be/W wall environment, as well as to provide sets of data across isotopes (H, D, H-D, T, D-T). In contrast, the DTE3 campaign was designed as an extension of JET's deuterium campaigns in 2022–2023 [12], which focused on developing scenarios for ITER and DEMO, integrating in-depth physics understanding and control schemes. The objectives were to demonstrate the feasibility of these scenarios when operating with a deuterium-tritium fuel mix, to obtain information on physics aspects dependent on the isotope mass within these scenarios and in other ITER- and DEMO-relevant conditions, to undertake studies only possible with operations with tritium such as on tritium retention, and to address open issues and questions arising from the analysis of experiments performed in DTE2.

The DTE3 campaign relied heavily on the knowledge gained and the work invested before and during the T and DTE2 campaigns in 2021–2022. The short time since the DTE2 campaign (less than two years, compared to 24 years between DTE1 and DTE2) meant that the experience with D-T fuel mix was still fresh for both the scientific and operations teams. Lessons learned from DTE2 could be implemented to DTE3 [14]. Differently to DTE2, the DTE3 experimental program was organised in sessions, similarly to how it is organised during D operations, allowing the simplification of the experimental scheduling and a more efficient exploitation of the experimental time available. Furthermore, both NBI injectors were operated in D, due to the lower reliability and additional constraints experienced in DTE2, where one of the two beam boxes was operated in T [15, 16]. Moreover, it was demonstrated in DTE2 that NBI fuelling in high power scenarios did not have any effect on the D/T ratio in the plasma [17]. As previously, the organisation of the scientific program and experiment preparation were optimised to make the most out of the limited experimental time with D-T fuel and to ensure the best scientific outcome while avoiding risks to the machine and to the rest of the scientific program. After DTE3 and a period of operations to reduce the tritium amount in the vessel, JET resumed D operations to complete the scientific program and to obtain deuterium pulses to serve as comparison references for the D-T pulses run in DTE3.

As in the previous D-T campaigns, budgets were imposed on the number of 14 MeV neutrons that could be produced and on the amount of tritium gas to be used. The 14 MeV neutron budget available for DTE3 was the amount leftover after those produced in the previous campaigns, up to the limit set in the JET safety case that allows a total of $2 \cdot 10^{21}$ 14 MeV neutrons over its lifetime [18, 19]. Following DTE2 which produced a total of 8.48×10^{20} 14 MeV neutrons, there was leftover budget allowing for the DTE3 experiments. The D-T experiments in DTE3 produced in total 7.31×10^{20} neutrons. The DTE2 and DTE3 campaigns together produced 86.8% of the JET lifetime D-T neutron budget. The tritium inventory available for experiments in DTE3 was 41.6 g (69 g were available for DTE2 and 21 g for DTE1 experiments). In DTE3, ∼117 grams of tritium were supplied to the Tritium Introduction Modules (TIMs) [20–22] (only deuterium NBI was used). Only part of this tritium is actually injected into the torus, as will be discussed in section 8. For reference, ∼100 g were used in DTE1 (∼35 g via the then single Tritium Introduction Module and ∼65 g to the NBI) and ∼1 kg in DTE2 (∼240 g via the Tritium Introduction Modules and ∼763 g to the NBI). A limit of 44 barl of tritium consumption per operational day was applied to the cryopump cryopanels, as in DTE2 [14].

The scientific objectives of the DTE3 campaign can be summarised as follows:

(i) Assess the impact of changing the plasma fuel from D to D-T on the Ne-seeded ITER baseline scenario, and characterise the core-edge-SOL integration in D-T in preparation for ITER (section 3)
(ii) Evaluate the effect of isotope mass change from D to D-T to T on peeling limited pedestals (section 4)
(iii) Explore conditions for peripheral impurity screening in hybrid scenario plasmas in D-T (section 5)
(iv) Demonstrate the feasibility of the Quasi-Continuous Exhaust regime, a candidate scenario for ITER and DEMO, in D-T, compare its characteristics with D, and assess the access to the QCE in D-T (section 6)
(v) Demonstrate the existence of the X-point radiator regime, suitable for full detachment in DEMO, in D-T and demonstrate the real-time control of full divertor detachment in D-T (section 7)
(vi) Continue the studies on tritium retention and tritium clean-up started in the T and DTE2 campaigns, including the use of new diagnostic capabilities, to inform ITER and future fusion devices (section 8)
(vii) Investigate nuclear technology issues in a tokamak environment in preparation for ITER (section 9)
(viii) Address outstanding issues from the T and DTE2 campaigns (section 10).

3. Development of a core-edge-SOL integrated scenario for ITER

The ITER baseline scenario is the reference scenario for ITER to achieve $Q = 10$ at a plasma current of 15 MA [23–25]. It is necessary that the scenario combines a high-performance core and pedestal plasma to achieve the target for fusion power production, and a partially detached divertor via impurity seeding to keep the heat loads on the divertor at a manageable level (<10 MW/m^2) to protect the divertor targets [26]. In preparation for ITER, efforts to develop a core-edge integrated scenario at JET with high confinement and with partially detached divertor conditions with the so-called JET ITER baseline scenario, were started just before DTE2. For these investigations, a plasma configuration close to the ITER shape is chosen, with a high triangularity $\delta_{\rm av} \sim 0.35 - 0.38$ and with the inner and outer strike legs on the vertical targets of the JET divertor. Neon or nitrogen are used as extrinsic impurities to achieve detachment (nitrogen seeding is not desired in D-T operations, due to the formation of tritiated ammonia [27] and in JET in particular due to concerns of poisoning the uranium beds storing the tritium). These core-edge integration studies have demonstrated that at 2.5 MA/2.7 T in deuterium, it is possible to obtain a Ne-seeded plasma with high-performance ($H_{98} = 0.9, \beta_{\rm N} = 2.2$), with high recycling divertor conditions. These conditions were sustained for 4 s without tungsten accumulation and without type-I ELMs [28, 29]. The scenario was also tested with D-T fuel in DTE2, demonstrating for the first time the impact of Ne-seeding on a plasma with a $n_{\rm D} \sim n_{\rm T}$ fuel mix [29]. However, the operational domain was limited for technical reasons allowing the input power to be only 23-25 MW instead of the anticipated 28 MW. As a result, high performance was not achieved in DTE2, but the key aspects of core-edge integration obtained in D was also observed in D-T (similar increase of performance and reduction of the ELM size with increasing Ne concentration). For clarification, the JET ITER baseline scenario discussed here is different to the so-called JET baseline scenario with low triangularity and a plasma configuration optimising pumping which was extensively developed for high fusion power production in the DTE2 campaign [10, 30].

In the D campaigns preceding DTE3, the investigations on the high-performance integrated scenario, started before DTE2, were continued placing the focus on expanding the operation domain towards lower pedestal collisionality, both with Ne- and with N-seeding, and on understanding the conditions in which ELMs are avoided [31, 32]. Beyond the scenario development efforts to simultaneously integrate the core and edge requirements, the main objective of these experiments was to provide the physics understanding of the core-edge-SOL integration. For this reason, particular attention was given to obtaining well-diagnosed plasmas (namely diagnostic measurements in the divertor, SOL, pedestal and core), to study in detail the core-edge integration at various fuelling and seeding levels and divertor conditions. These data can be used to validate core and edge modelling predictions, as well as integrated modelling codes aimed at describing the plasma from the core to the divertor. Higher levels of heating power $P_{\rm in} \sim 33 - 37$ MW ($P_{\rm NBI} \sim 28 - 32$ MW and $P_{\rm RF} \sim 5$ MW) were now available. The plasma current was increased from moderate (2.5 MA) to higher values (3.0 – 3.2 MA), at $q_{95} \sim 2.7 - 3.3$, something never attempted before with a high-triangularity shape with the JET-ILW. However, operation at high current was technically very challenging [33]. Nitrogen or neon seeding was shown to lead to high recycling or even partial detachment at the outer divertor. Conditions avoiding strong type-I ELMs, and completely avoiding ELMs with larger impurity concentrations, were regularly achieved. The scenario was pushed to higher confinement ($H_{98} > 0.8$) and lower pedestal collisionality $\nu^*_{\rm e,ped}$ down to ~ 0.5 (calculated based on equation (18b) from [34]), approaching the values of 0.1-0.2 expected in ITER. The scenario development efforts and challenges and the detailed plasma characteristics are elaborated in [31, 32]. Notably, in Ne-seeded deuterium plasmas, H-mode operation could not be sustained at 3.2 MA/3.45 T, even with $P_{\rm in} \sim 37\,MW$, while the plasmas at 3.0 MA/2.9 T had only modest normalised confinement. This is at least partially attributed to the technical difficulties of high current operation and the limited heating power available.

In DTE3, the ITER baseline scenario development aimed to demonstrate how the scenario properties and the core-edge-SOL integration solution are modified when the plasma fuel is changed from D to D-T ($n_{\rm D} \sim n_{\rm T}$). Considerable effort has been made to provide this information for two plasma currents, namely 2.5 MA and 3.0 MA, with Ne-seeding, despite the technical difficulties at high current. The impact of extrinsic seeding impurities compatible with D-T ITER operation was studied (Ne, as N was not an option in DTE2 and DTE3). High-performance plasmas were achieved in D-T at 2.5 MA, with $\beta_{\rm N}$ reaching 2.5. Remarkably, the Ne-seeded deuterium-tritium plasmas have a much higher performance at 3.0 MA/2.9 T than the corresponding deuterium plasmas at 3.0 MA and 3.2 MA, and also low target temperatures and small or no ELMs. This indicates that the changes in the plasma behavior due to the different isotope mass in D-T are beneficial compared to D. Furthermore, the importance of the D-T operation is highlighted in this case as it has allowed the study of the effect of extrinsic impurities (Ne) on the divertor, SOL and pedestal, at two different plasma currents. Analysis is ongoing to elucidate the physics reason for the easier access to high performance in D-T with respect to D.

As a result, a high-performance (stored energy ~ 8 MJ, $H_{98(y,2)} \sim 0.85$) neon seeded ($c_{\rm Ne} \sim 2.2\%$) integrated scenario with a partially detached divertor could be demonstrated at 3.0 MA/2.9 T with D-T fuel and $P_{\rm NBI} \sim 30$ MW and $P_{\rm RF} \sim 5$ MW [31–33, 35]. The scenario is stationary for a long time (>7 s), without tungsten accumulation and even without type-I ELMs. The best performing D-T pulse is shown in figure 1. Due to a tight experimental schedule, no specific focus was placed on increasing the fusion power produced in this scenario, ~ 4.0 MW of fusion power were produced in this pulse. The fusion energy of this pulse is 27 MJ, which exceeds the highest fusion energy achieved with ELMy

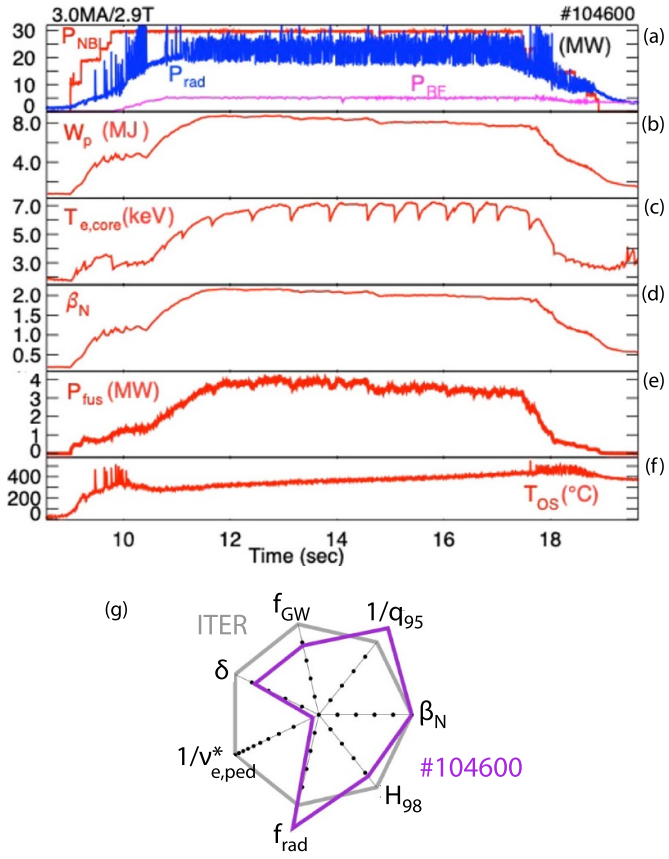

Figure 1. Time traces of JET pulse #104600: a high-performance, partially detached, Ne-seeded ITER baseline scenario pulse in D-T ($n_D \sim n_T$) at 3.0 MA and 2.9 T. The ITER-like plasma shape with high triangularity and the strike points on the vertical target is used. (a) Heating and radiated power, the latter showcasing the avoidance of W accumulation and lack of type-I ELMs, (b) stored energy ($H_{98(y,2)} \sim 0.85$), (c) core electron temperature, (d) normalised pressure β_N, (e) the produced fusion power, (f) tile temperature at the outer strike point, showcasing the reduced temperature at the target and the lack of type-I ELMs. (g) The key parameters of this pulse (purple) are compared with those of ITER (grey, quoted here in brackets) [37], namely $H_{98(y,2)} = 0.85$ (1.00), $f_{GW} = 0.65$ (0.85), $q_{95} = 2.7$ (3.2), $\beta_N = 2.0$ (2.0), $\nu^*_{e,ped} \sim 0.51$ (0.06), $\delta = 0.36$ (0.47), $f_{rad} = 0.94$ (0.75) (the radiated fraction of #104600 is corrected to obtain power balance, following [38], the ratio of the signals as shown in (a) being $P_{rad}/(P_{NBI} + P_{RF} + P_{Ohm}) \sim 0.65$).

H-modes in DTE1 (22 MJ) [7], though with higher input power (see figure 7). The performance and fusion energy of the seeded ITER baseline D-T pulses is a remarkable achievement considering the use of extrinsic radiating impurities and the high fuelling gas rate in these pulses. These pulses should be additionally compared with the ITPA20-IL scaling [36], which is more suitable for scenarios with strong shaping and higher density operation, though it is also not applicable to seeded plasmas. In addition, an extensive set of pulses in steady conditions has been achieved at various fuelling rates, in partially detached conditions, with and without ELMs, at both lower (2.5 MA) and higher (3.2 MA) current. Detailed analysis of this comprehensive data set is underway, to understand the confinement improvement observed with Ne-seeding, the resilience of the pulses to W accumulation, and the impact of Ne-seeding on pedestal transport and stability, near and far SOL transport, core plasma transport and divertor conditions. Core and edge modelling codes will be compared with the datasets in both D and D-T, and integrated modelling will be carried out with the aim of increasing the reliability of predictions for ITER.

4. Investigation of peeling limited pedestals

ITER will operate at low collisionality ($\nu^*_{e,ped} < 0.1 - 0.2$), with a low density gradient at the pedestal and a high ratio of separatrix to pedestal electron density, and as a consequence the pedestal may be limited by peeling instabilities (modes with $n \sim 1 - 5$) [39, 40]. Peeling-limited pedestals have been achieved so far in DIII-D [40] and TCV [41], but machines with a metal wall such as ASDEX Upgrade and JET typically operate at the ballooning boundary. In plasmas where ELMs are triggered by ballooning modes ($n > 20$), confinement is found to degrade with increasing pedestal electron density, and with increasing n_e^{sep}/n_e^{ped} [42, 43]. Dedicated experiments prior to the DTE3 campaign investigated peeling limited plasmas in JET in deuterium [44, 45], aiming to compare the physics of peeling-limited and ballooning-limited pedestals and to test the predictive modelling capabilities for peeling-limited pedestals. As the effect of changing the isotope mass from D to D-T to T on the pedestal has previously been studied for ballooning-limit pedestals [46, 47], plasmas with a peeling-limited pedestal were also run with a deuterium-tritium fuel mix in DTE3.

EUROPED [48] predictions have shown that reaching low $\nu^*_{e,ped}$ is not sufficient for the pedestal to be limited by peeling modes, rather, higher q_{95} is additionally required to achieve peeling-limited pedestals in the range of densities that are achievable in the JET-ILW. A high triangularity scenario ($\delta_{av} \sim 0.37$) was chosen to relate with the ITER shape. To allow for low plasma density, a low plasma current of 1.4 MA and a low gas rate ($0 - 1 \times 10^{22}$ e/s) were chosen, and additionally the outer strike point was placed near the throat of the cryopump, to maximise the pumping efficiency. The heating power was $P_{NBI} = 22 - 25$ MW and $P_{RF} \leqslant 3$ MW. High B_T of 3.4 T and 3.8 T was used, corresponding to $q_{95} = 7.5$ and 8.2, respectively. With respect to the pedestal top values previously achieved and reported in the JET-ILW database [43], these pulses reached values never achieved before, namely higher T_e^{ped} values, with n_e^{ped} lower than all other high-δ pulses in the database. Furthermore, lower $\nu^*_{e,ped}$ values where achieved at a similar range of n_e^{sep}/n_e^{ped} with respect to the aforementioned database. A positive dependence of the pedestal electron pressure on the electron density was observed in these plasmas in deuterium [44, 45], a behavior opposite to that commonly

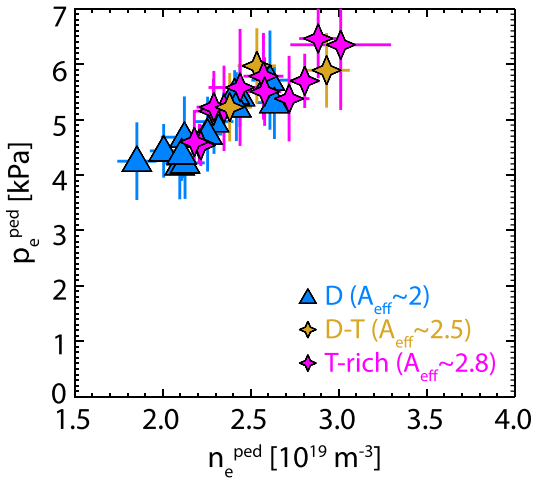

Figure 2. Positive dependence of the electron pressure with the electron density at the pedestal top for deuterium (blue triangles), deuterium-tritium (gold stars), and T-rich (magenta stars), high q_{95}, high triangularity pulses (1.4 MA/3.8 T, $q_{95} \sim 8.2$, $P_{in} \sim 25$ MW) with a peeling-limited pedestal.

observed in ballooning-limited pedestals [42, 49], consistent with what has been observed in peeling limited pedestals in DIII-D and in EPED predictions [50], indicating that the pedestals are limited by peeling physics. EUROPED modelling indicates that the most unstable modes are peeling modes, and good qualitative agreement with the experimental results is found [44, 45].

The most promising plasmas obtained in pure D plasmas at 3.8 T (highest q_{95}) were then repeated with mixed D-T fuel ($n_D \sim n_T, A_{eff} \sim 2.5$) and with a majority tritium concentration (T-rich plasmas, $A_{eff} \sim 2.8$), to study the effect of higher isotope mass on the peeling limited pedestals. The pulses were performed in $n_D \sim n_T$ and in T-rich fuel, and fuelling rate scans ($0.1 - 1 \times 10^{22}$ e/s) at constant power were performed. Figure 2 shows the positive dependence of the pedestal electron pressure on the electron density which was also observed in D-T and T-rich pulses, as in D, indicating that these pedestals at high q_{95} are also limited by peeling physics, which is also confirmed by preliminary modelling. With the addition of tritium, an increase in n_e^{ped} and p_e^{ped} is observed with increasing A_{eff}, similar to what was observed for ballooning limited pedestals [46, 47]. The detailed analysis of the D-T and T-rich pulses has shown that there is no direct effect of the isotope mass on the pedestal stability, but rather an indirect effect via the isotope effect on the density; the higher isotope mass results in a higher pedestal density, leading to improved stability at the peeling boundary and higher pressures [45]. Notably, while the effect of isotope mass on pressure is similar to that in ballooning-limited pedestals, the underlying origin of the effect is different. This work improves the understanding of peeling-limited pedestals and informs the pedestal modelling for ITER predictions.

5. Peripheral impurity screening

Keeping tungsten out of the plasma core is critical to minimise high radiation losses and plasma cooling; furthermore, an increased tungsten concentration also limits the parameter space in which ignition can be achieved [51]. A low tungsten content in the plasma core can be achieved by screening the tungsten at the plasma edge if the ion temperature gradient is strong enough with respect to the electron density gradient, leading to outward neoclassical convection of tungsten [52, 53]. This 'temperature gradient screening' has been predicted for ITER conditions [54, 55]. Impurity screening in the plasma periphery was experimentally observed for the first time in optimised hybrid scenario deuterium plasmas (Type-I ELMy H-mode) in JET [56], with similar observations in DTE2 [57]. The screening strength was found to be enhanced by the strong rotation and low collisionality of these plasmas [58]. Further investigations on this topic have been carried out in deuterium and in DTE3 to narrow down the location across the pedestal in which the impurity screening is observed and to qualify the ELM and inter-ELM dynamics of impurity transport in a wider range of parameters.

The key element in achieving tungsten screening conditions in the hybrid scenario plasmas has been the optimisation of the fuelling at the beginning of the heating phase [57] both in terms of fuelling rate and timing to achieve the conditions required for impurity screening, namely low n_e^{ped}, high T_i^{ped}, high P_{in}, low collisionality and strong rotation. In D, a density variation was performed by varying the fuelling rate and timing, and the plasma current (lower plasma currents compared to the 2.3 MA studied in [56] down to 2.1 MA). Tangential NBI injection was also used to vary the plasma rotation, though with a limited effect [59–61].

In DTE2, the studies were hampered by the fact that the horizontal bolometry camera, a critical measurement for the analysis of the tungsten behavior, was affected by the tritium fuelling from a nearby main chamber TIM (which led to increased measured signals for several of its lines-of-sight) [57] and special efforts were made to avoid this in the DTE3 experiments. In DTE3, only a divertor TIM was used for the tritium fuelling in the flat-top to avoid compromising the horizontal bolometry camera measurements. Pulses that completely avoided the use of the main-chamber TIM were also obtained to ensure no effect on the data. To compensate for the use of deuterium-only NBI in DTE3, the pulses were designed to be T-rich in the current ramp-up. By tuning the H-mode entry as described in [57], a very good match with the deuterium pulse #97781, in which the

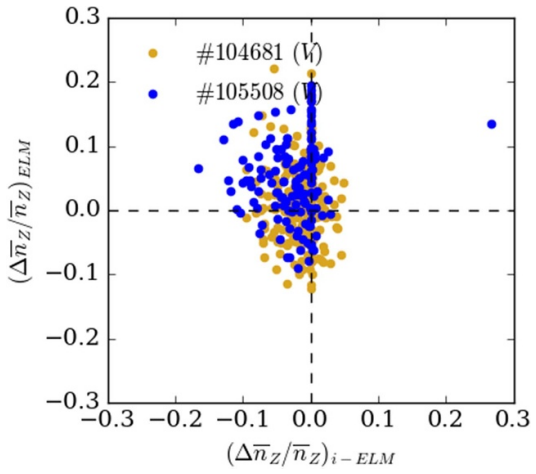

Figure 3. Relative change of the W content in the plasma due to ELM flushing (y-axis) versus that due to inter-ELM influx (x-axis) inferred from the measurements from the vertical bolometry camera. A D-T pulse (#104681) and a D pulse (#105508) are compared, shown in gold and blue points, respectively. Positive and negative changes indicate an inward and a outward transport direction, respectively. A comparison between cases with and without screening is presented in [56].

impurity screening behavior was most clearly demonstrated, was achieved in terms of radiated power and edge parameters. Further improvement was achieved by increasing the magnetic field to 3.85 T, as this increased the L-H power threshold allowing the same heating power ramp as used in D plasmas without entering H-mode too early, and a very high pedestal top ion temperature of 4 keV was reached in the D-T pulse #104681 at 3.85 T/2.1 MA, $P_{\mathrm{NBI}} \sim 35$ MW, $P_{\mathrm{RF}} \sim 3$ MW and without main chamber tritium fuelling.

The detailed analysis of the bolometric measurements of the radiated emmissivity of the recent deuterium pulses at lower plasma current (2.1 MA) shows a similar or even improved screening behavior with respect to the pulse #97781 (2.3 MA) [56]. The D-T pulses also exhibit impurity screening behavior, but not as strong as the D pulses. In figure 3 the change in tungsten content in the D-T pulse #104681 and in the D pulse #105508 due to ELM flushing is compared with that due to the inter-ELM influx. In both pulses the radiation is at low levels and remains controlled, but the radiation fraction is much lower in the D pulse ($\sim 20\%$ compared to $\sim 30\%$ in the D-T pulse). In both pulses, tungsten is shown to be moderately screened between ELMs. In the D pulse, on average the ELMs cause an influx rather than expulsion of impurities, while in the D-T pulse their effect is neutral. However, the D pulse shows stronger screening behavior. Modelling of the recent D and D-T pulses with FACIT [62] and NEO [63–65] is underway to assess the role of neoclassical transport in the observed impurity screening across the pedestal gradient region [61]. The elucidation of the transport processes under these conditions by modelling will be a valuable input for ITER, especially in view of the recent decision to operate ITER with a full tungsten wall.

6. Development of the quasi-continuous exhaust small-ELM regime

Operating scenarios considered for DEMO should offer a solution for power exhaust, but also ensure the avoidance of transiently too high energy loads due to ELMs and good performance for fusion power production. The Quasi-Continuous Exhaust (QCE) regime developed in ASDEX Upgrade [66, 67] and TCV [68] is a promising, naturally type-I ELM-free scenario. The QCE regime operates at high density, which is beneficial as high separatrix density is a requirement for power exhaust, and showcases performance comparable to type-I ELMy H-mode scenarios [69]. Both high fuelling and strong shaping are necessary to achieve QCE. Frequent, low-amplitude filaments are present in place of ELMs.

The QCE has been extensively studied in ASDEX Upgrade and TCV, and an in-depth understanding of the physics governing the QCE behavior has recently emerged. The role of the separatrix and in particular of ideal ballooning modes becoming unstable at the pedestal foot has been highlighted as explanation for the avoidance of type-I ELMs [67, 70]. The collisionality and the related turbulence control parameter α_t, defined in [71], in this region has also been connected to the transition to QCE. Furthermore, QCE access criteria have been developed based on an ideal MHD model, namely the minimum shaping and separatrix density required [72]: stronger shaping allows the local ideal ballooning modes to destabilise before global modes can become unstable, and the high separatrix density increases the pressure gradient at the pedestal foot allowing the local ballooning modes to become unstable.

This understanding and the experience gained in AUG and TCV motivated the investigation of the QCE regime in JET. JET's larger size helps in reducing the pedestal top collisionality at a given separatrix collisionality. Furthermore, JET's tritium capability offers the possibility to investigate the regime in mixed isotope plasmas, to demonstrate its feasibility in deuterium-tritium mixed plasmas, and to identify any differences in the QCE behavior and access requirements between D and D-T plasmas. As described in section 2, one of the main goals of the DTE3 campaign was to assess scenarios for power exhaust, naturally including the QCE regime.

The QCE regime was successfully ported to JET in deuterium plasmas [73, 74]. Initially, the shaping requirement was addressed by developing a close-to-double-null shape, building on the shape developed in [75]. With this strong shaping, sufficient heating power to stay clearly in H-mode and sufficient fuelling (i.e. high enough separatrix density) to suppress the ELMs, stationary pulses in the QCE regime were obtained. As in the other devices, the characteristic high frequency filaments were observed also in JET. The aim to lower the pedestal collisionality with respect to the values achieved in smaller devices was met with $\nu^{*\mathrm{JET}}_{\mathrm{e,ped}} \sim 0.7 - 2.0$, lower than that achieved in the medium-size tokamaks $\nu^{*\mathrm{AUG}}_{\mathrm{e,ped}} \sim 1.6 - 25$ and $\nu^{*\mathrm{TCV}}_{\mathrm{e,ped}} \sim 2.6 - 17$, at similar pedestal top densities for JET and AUG as those predicted for ITER and EU-DEMO [73]. The collisionality $\nu^{*}_{\mathrm{e,ped}}$ quoted here is calculated based on

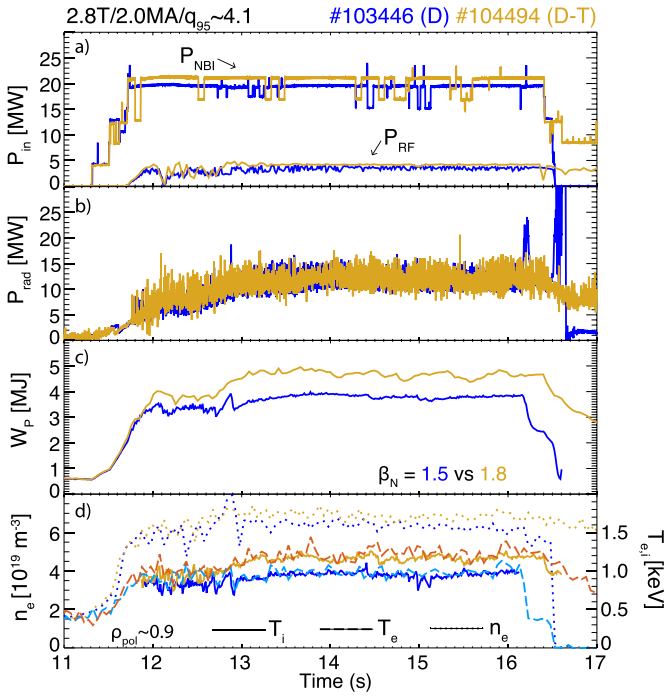

Figure 4. Comparison between two JET pulses in the QCE regime, one in deuterium (#103446 in blue) and one in deuterium-tritium mixture (#104494 in gold). (a) Input NBI and ICRH power, (b) radiated power, (c) stored energy, (d) electron density (· · · · · · · · ·) and electron (- - -) and ion (——) temperatures at $\rho_{\rm pol} \sim 0.9$. Both pulses have the same plasma shape ($S_{\rm d} \sim 5.3$ [72]), very similar filamentary behavior and reduced divertor power loads [74].

equation (18b) from [34]. The experimental observations and the required shaping and fuelling needed to achieve the QCE regime in JET are in line with the physics picture obtained in AUG and TCV [74] and further analysis will confirm whether the same physics mechanisms govern also the JET experiments.

The QCE regime was then straightforwardly operated with a deuterium-tritium fuel mixture. The QCE behavior was found to be similar in D-T, with regards to the access requirements for strong shaping, fuelling and heating and the filamentary behavior. The similarities between the QCE pulses in D and in D-T are not surprising, but rather confirm the expectations with changing the plasma effective mass, as the explanation based on ideal MHD does not indicate a mass dependence [72], and the mass dependence of the power fall-off length is weak [69]. The parameter space in which QCE was achieved in D-T is a subset of that achieved in D, for example QCE pulses were achieved with a plasma current up to 2.0 MA in D-T while 2.25 MA were achieved in D. However, it should be stressed that this was simply to the limited experimental time available to work with D-T plasmas, rather than any other limitation of the scenario. Overall, the boundaries of the QCE existence parameter space both in D and D-T were mainly due to technical constraints, rather than physics reasons limiting the QCE regime.

Figure 4 shows a comparison between a D and a D-T QCE pulse. The plasma shape is identical between the two pulses (close-to-double-null), and the gas fuelling very similar. The deuterium-to-tritium ratio is $n_{\rm D} \sim n_{\rm T}$, slightly varying from D-rich to T-rich during the pulse. With only slightly higher input power, significantly higher stored energy and normalised pressure is observed in the D-T pulse ($\beta_{\rm N}^{\rm D} \sim 1.5$ and $\beta_{\rm N}^{\rm D-T} \sim 1.8$). This originates from a higher pedestal pressure in D-T, phenomenologically similar to observations in type-I ELMy H-modes in D-T [46, 47]. However, in the QCE pulses, the increase in pressure is due to higher pedestal electron and ion temperatures and electron density in D-T, contrary to the observations in other plasma scenarios where the increased pressure is predominantly due to a higher electron density. The pedestal collisionality of the D-T pulse is lower than that of the D pulse ($\nu_{\rm e,ped}^{*\rm D} \sim 1.2$, $\nu_{\rm e,ped}^{*\rm D-T} \sim 0.9$).

The QCE pulses in DTE3 have proven that the QCE regime can be achieved in D-T plasmas. As discussed, producing a high level of fusion power was not the goal of these experiments. Rather, it was successfully shown that there are no differences in D-T in terms of the QCE access criteria and overall characteristic QCE behavior such as the absence of type-I ELMs. The detailed analysis of the transport, confinement and mode stability in the D-T plasmas will allow the inclusion of the role of the isotope mass in the physics understanding of the QCE regime.

7. The X-point radiator regime

A future power plant will need to operate with a detached divertor to protect the first wall materials from the very high heat and particle loads. More than 95% of the exhaust power should be dissipated, with a large fraction thereof dissipated in the confined region. With this in mind, fully detached scenarios and their characteristics have been actively investigated. Impurity seeding is used to increase the radiated power and induce detachment. With the pronounced detachment of the outer divertor induced by impurity seeding, a small region with intense radiation, low temperature and high density evolves inside the confined plasma at or slightly above the X-point. This so-called X-point radiator has been observed in ASDEX Upgrade and JET [76, 77], as well as in many other tokamaks [78]. The X-point radiator regime (XPR) was shown to be a stable operational scenario that offers access to complete detachment with various seeding impurities, and can even provide conditions in which ELMs are suppressed. An analytical model for the XPR has been developed in [79]. Additionally, it was demonstrated at ASDEX Upgrade that the XPR position above the X-point can be controlled in real-time, providing a way to control the full divertor detachment [80].

In the recent JET deuterium campaign preceding DTE3, the XPR scenario has been investigated further at higher input powers (up to 33 MW) with respect to previous investigations [78], and also mixes of impurities were used for seeding (combinations of nitrogen, neon and argon). With these improvements, the XPR regime was further stabilised and an active control for the XPR position was implemented. The scenario investigations were performed at (for JET) moderate plasma current and magnetic field (2.5 MA/2.65 T), usually

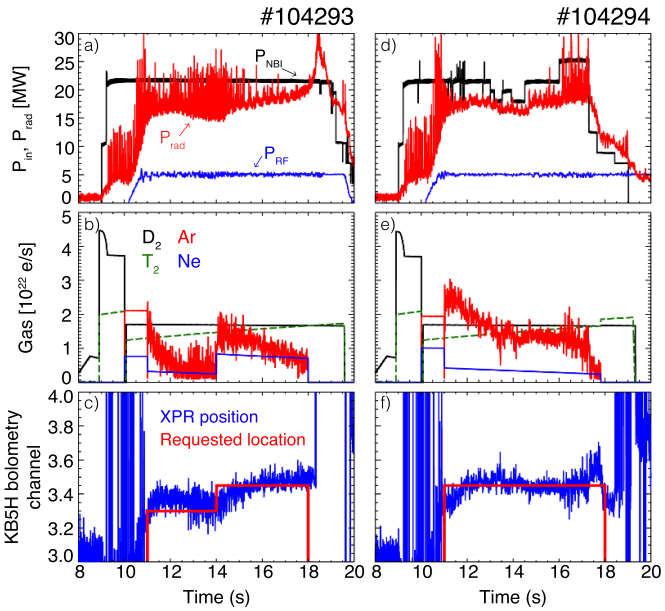

Figure 5. Two JET D-T pulses in which the height of the X-point radiator is controlled in real-time by controlling the argon seeding in feedback, while Ne is injected in feed-forward. In #104293 the XPR position is successfully controlled at two different heights and in #104294 the XPR position is successfully maintained despite a perturbation in the input heating power. (a) Heating and radiated power, (b) gas flow requests and (c) the XPR position defined by the bolometry channels of the horizontal JET bolometry camera for #104293, (d)–(f) for #103294, respectively.

at medium to high input power ($P_{\text{in}} \sim 25 - 27$ MW) and with a low triangularity plasma shape. The XPR control method developed in ASDEX Upgrade was successfully ported to JET [81, 82]. As in ASDEX Upgrade, the XPR position was detected in real-time using bolometry signals and was controlled in real-time using impurity injection.

The existence of the X-point radiator was demonstrated also in D-T plasmas in stationary conditions and was also successfully controlled in real-time. The dynamics of the XPR position control were almost identical between D and D-T. The availability of a real-time control scheme helped to quickly obtain similar conditions in D-T plasmas as in D plasmas. A mixture of argon and neon seeding was used in D-T as this was identified to be the best choice in D plasmas, while maintaining the compatibility with D-T operations, since nitrogen seeding is not an option (due to the formation of tritiated ammonia). Plasmas seeded with an argon and neon mix performed better than single impurities and stayed reliably in H-mode (unlike the plasmas with single seeding species) [78]. Two example pulses are shown in figure 5: the XPR position is successfully controlled to two different heights in #104293 and the XPR position is kept to a set level despite a strong perturbation in the input heating power in #104294 (which would have otherwise affected the XPR position) by seeding argon in feedback and neon in feed-forward mode.

As in deuterium plasmas with relatively high power and argon and neon seeding mixture, the presence of the XPR did not have a detrimental impact on the plasma confinement in D-T once it is ensured that the H-mode is maintained with sufficient heating power and the appropriate seeding mix. In particular, no strong deterioration of the edge pressure was observed with the introduction of impurity seeding. The core temperatures increase with the seeding (the ion temperature more strongly so than the electron one), following past observations in such seeded scenarios, explained by the stabilisation of ITG modes in the plasma core [83]. It should be stressed here that the confinement in the pulses investigated to address the XPR physics and control is low ($H_{98(y,2)} \sim 0.65$ for unseeded and $H_{98(y,2)} \sim 0.7 - 0.8$ for seeded deuterium plasmas). As these pulses involve strong impurity seeding, they are not appropriately described by the existing confinement scalings. Due to the limited run time available, there were no efforts invested in achieving high confinement in this seeded scenario, neither in D nor in D-T plasmas.

Comparing seeded D-T and D plasmas with an XPR present (with argon and neon seeding), the changes due to the different plasma effective mass are in line with previous observations [46, 47]. The stored energy in the D-T plasmas is higher with respect to the D ones, with a higher electron density in D-T (across the plasma radius), while the electron and ion temperatures are similar. Demonstrating high fusion power production and high performance was outside the scope of the D-T experiments in this scenario, which aimed at demonstrating the existence and control of the XPR in D-T, and at confirming that the XPR regime is achievable also in the relevant fusion fuel. The applicability and performance of the XPR regime in ITER and future fusion power plants still needs to be investigated [78], and the experiments in D and D-T at JET provide unique data for this purpose. Detailed modelling, among others with SOLPS-ITER and integrated modelling, is underway to improve the understanding of the XPR as well as the predictions for such regimes and their confinement in future devices.

8. Tritium retention and clean-up

The retention of the fusion fuel in the plasma-facing components is one of the main concerns for ITER and future fusion power plants. High levels of retention in the wall would imply high levels of radioactivity in the first wall materials, adding to those produced due to the neutron activation, with implications for machine decommissioning. The tritium stored in different regions of the vessel should be limited to comply with safety regulations. During operations, excessive tritium retention would mean that operations cannot continue until the tritium inventory is reduced below the safety limits. In addition, high tritium retention limits the amount of tritium that can be used to fuel the plasma, placing additional demands on the tritium breeding ratio in fusion power plants. Therefore, the quantification of the fuel retention and the characterisation of the tritium cycle is crucial information for ITER and any future fusion device.

Understanding fuel retention has been a major activity at JET since it was recognised that the tritium retention in the JET carbon wall following the PTE and DTE1 campaigns was unacceptable [84, 85]. The change to a metal wall for JET was

motivated by these results and the deuterium fuel retention with the JET-ILW was found, as expected, to be significantly lower [86, 87].

JET provides a unique opportunity for such studies in a fusion device environment and in particular with a large tritium inventory as discussed in section 2. The amount of tritium injected into the vessel, which is the relevant number for retention studies, was 107.5 g in DTE3 (only via the TIMs). For reference, 145.2 g were injected into the vessel in DTE2 (138.8 g via the TIMs and 6.4 g via the NBI), and 106.7 g in the T campaign (96.5 g via the TIMs and 10.2 g via the NBI) [88]. Studies to assess tritium retention and tritium removal were performed in DTE3 [88, 89], to extend the work done before, during and after the DTE2 and T campaigns in 2021-2022 [90, 91]. A variety of fuel retention measurements were obtained in DTE3, addressing both global and local retention.

The global retention is derived from in-vessel gas balance measurements [86, 92], by assessing the gas and particle balance between the injected and the recovered fuel after a pulse (short term) or after several identical pulses (long-term retention), or after longer operating periods. This technique is particularly challenging as it is associated with large uncertainties when retention levels are low (as is the case in JET-ILW). The tritium accounting following the DTE2 and T experiments was unfortunately inconclusive [91]. This also became clear in DTE3, where so far only a qualitative assessment was possible from the gas balance measurements obtained via the Residual Gas Analysis and Pressure Volume Temperature technique [91]. The preliminary analysis based on these measurements indicated that there is no significant isotope effect on the global in-vessel fuel retention, when comparing D_2, T_2 and D-T plasmas [89], with no significant difference observed within the accuracy of the technique. Further work is required to confirm the independence of fuel retention on the fuel mass, including a comparison of the short and long-term retention and outgassing observed.

In addition to the challenging gas balance measurements, the local in-situ fuel retention was measured for the first time using a unique diagnostic based on Laser-Induced Desorption Quadrupole Mass Spectrometry (LID-QMS) [93]. Following its commissioning in the deuterium experiments preceding DTE3 in 2023, the LID-QMS provided the first-ever in-situ tritium retention measurements in DTE3. The LID-QMS laser was directed at the uppermost tiles of the inner divertor (Tile 0 and Tile 1, see figure 1 in [90]), where retention by co-deposition is high in the JET-ILW [90]. The LID-QMS was shown to have sufficient sensitivity to measure the desorbed fuel and to distinguish between D_2, DT and T_2, see figure 6 [93], allowing qualitative comparisons of the relative changes in fuel retention [89]. The LID-QMS measurements are in qualitative agreement with the fuel retention predictions which estimated that ∼2% of the injected fuel is retained in-vessel, based on gas balance measurements [86] and the distribution of retention in the vessel based on post-mortem analysis of vessel wall tiles [90, 94]. The quantitative analysis of the LID-QMS measurements is ongoing and calibration methods for the diagnostic are being developed [95].

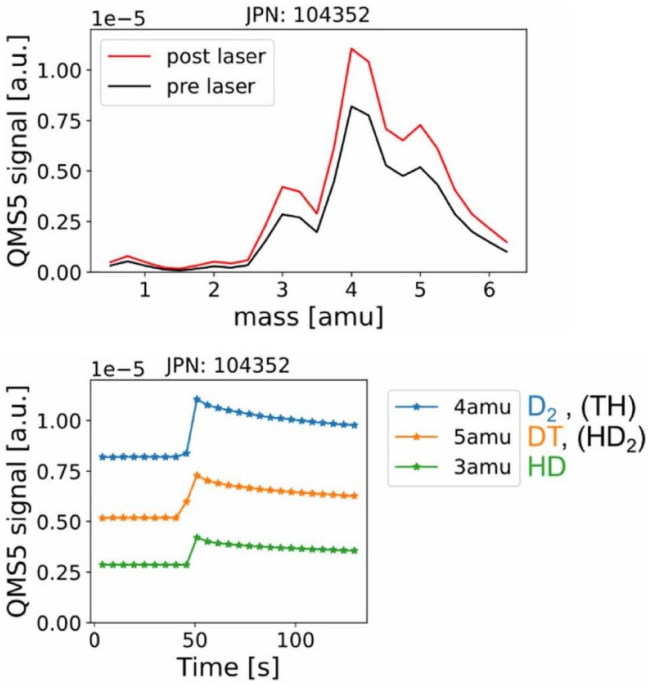

Figure 6. LID-QMS spectra (left) and time traces (right) obtained before and after gas was desorbed due to the LID-QMS laser pulses on the tile, illustrating that the diagnostic has sufficient sensitivity to distinguish between D_2, DT and T_2. The fuel retention is measured in-vessel after one week of JET D-T plasma operations. The gas is desorbed with 99 separated laser spots in raster mode. The laser spot has 3 mm diameter and the pulse rate is 50 Hz resulting in the desorption of fuel from an area of 7 cm^2 in 1.98 s. The laser power was 21 kW and the pulse length was 1 ms. Reproduced from [93]. © 2024 The Author(s). Published by IOP Publishing Ltd on behalf of the IAEA. CC BY 4.0.

After the end of JET operations in 2023, the LID-QMS and global gas balance measurements is being complemented by Laser-Induced Breakdown Spectroscopy (LIBS) measurements [96], a new diagnostic utilised now that the JET vessel is vented. In addition, ex-situ post-mortem analysis of plasma-facing component samples after removal from the JET vessel will be performed, as was done following the first JET-ILW deuterium operations in 2011–2016 [90, 94, 97, 98]. The removed plasma-facing components will include the tiles that were used for in-vessel LID-QMS fuel retention measurements to allow for a comparison with ex-situ retention measurements.

Both the DTE2 and DTE3 campaigns were followed by specially designed, optimised tritium clean-up operations, including both plasma operations and other techniques. Several methods were tested prior to and after DTE2, and subsequently applied also in DTE3 to assess their effectiveness in removing tritium from the JET vessel, as was done after T and DTE2 operations in 2021/2022 [91]. The cleaning after DTE3 included baking the vessel to 320 °C, also in combination with ion cyclotron wall conditioning, followed by limiter plasmas, raised inner strike point (with one strike point on Tile 1) plasmas [99] with NBI and RF heating, helium plasmas, and

specially designed clean-up plasmas with various heating configurations (some of which were also used for other scientific purposes). Throughout the tritium clean-up operations, regular LID-QMS measurements were carried out to provide information on the effectiveness of each method in removing T from the surfaces [88]. The detailed analysis to draw firm conclusions on the effectiveness of each method is still ongoing.

The objectives of the tritium clean-up were the reduction of the tritium concentration in the plasma below 1% to allow returning to D plasma operations with low neutron rates, and the reduction of the tritium content in the exhaust gas below 0.02% to be able to return the Active Gas Handling System (AGHS) system into standard operation without tritium. For the first objective, a combination of spectroscopic methods was used to assess the T concentration (optical Penning gauge spectroscopy in the plasma exhaust gas, spectroscopic Balmer lines measured in the divertor) as well as neutron measurements to indirectly infer the tritium concentration [91]. For the second objective, information from the exhaust gas analysis from AGHS and from the Exhaust Detritiation System were used. The trends were similar to those after DTE2 and about 4 weeks of operation were needed to reduce the tritium to the target value of 0.02%. The local fuel inventory in different areas of JET tiles was monitored extensively and regularly with LID-QMS throughout the DTE3 campaign, the tritium clean-up phase and the subsequent deuterium experiments.

Despite the challenges, significant progress was made in understanding tritium retention and clean-up. New diagnostics (LID-QMS) and clean-up procedures were developed. Given the technical difficulties in achieving quantitative tritium accounting, important lessons have been identified on how to address fuel retention in future devices. Specifically for gas balance measurements, contamination of the exhaust gas due to technical issues or preceding plasmas can lead to unacceptably high uncertainties in its characterisation and needs to be avoided. For LID-QMS, quantitative analysis requires understanding of pumping conditions which necessitates a gas injection calibration system [93]. The lessons learned from these experiments underscore the importance of implementing dedicated in-situ gas balance instrumentation and the careful application of the technically challenging techniques required to quantify the tritium inventory [88].

9. Nuclear technology studies in preparation for ITER

In addition to plasma physics studies, the D-T operations at JET provide a unique opportunity to study nuclear technology issues in a tokamak environment. During the DTE2 and DTE3 campaigns, the total neutron fluence on the plasma-facing components of JET is of the order of 10^{16} neutrons$/\mathrm{cm}^2$. In comparison, the maximum neutron fluence expected at the front ITER shield block is five orders of magnitude higher at the end of its operational life and three orders of magnitude higher at the end of the first DT phase. Thus, the JET conditions cannot reach the same level of material damage or activation as those in the most-irradiated components of ITER machine. However, the neutron fluence levels reached at JET are comparable to those in middle port plugs and rear blanket regions of ITER at the end of the first DT phase, and in the rear port plugs at the end of its operational life. These regions house diagnostics and components of heating systems, making the JET conditions relevant in terms of cumulative fluence for these systems. Furthermore, due to the greater attenuation of radiation by ITER structures compared to JET, the shutdown dose rates in maintenance areas of JET are similar to those in ITER. More details can be found in [100, 101].

The technological exploitation of the JET D-T operation in preparation for the ITER nuclear operations was continued in DTE3, with the aim of improving the knowledge of nuclear technology and safety, and advancing the understanding of neutron irradiation. Considerable effort has been invested in the development and verification of neutron diagnostic calibration methods for 14 MeV neutron measurements. Accurate calibration of neutron detectors is essential to measure fusion performance and plasma parameters, to reduce the uncertainty margin in the use of the available neutron budget, and to provide accurate neutron yields for neutronics benchmark experiments. Absolute calibration of the main JET neutron diagnostics, i.e. the fission chambers (time-resolved neutron yield rate measurements) and the activation foils system (integral neutron yield) was performed in 2017 using a 14 MeV neutron generator deployed inside the vacuum vessel using the remote handling system [102]. The 14 MeV neutron calibration was verified during plasma operation in DTE2 and now also in DTE3, meeting the challenging ITER requirement of $\pm 10\%$ uncertainty. Further to neutron calibration, DTE2 and DTE3 projects included the characterisation of the activation and radiation damage to ITER functional materials, the validation of neutron streaming and shutdown dose rate modelling, and the development of detectors for test blanket modules. Key elements of these investigations are the development and validation of nuclear computational tools and experimental techniques, and the demonstration of the reliability of the codes used for ITER nuclear analysis. A detailed overview of the studies contributing to the preparation of ITER nuclear operation can be found in [103].

New studies were undertaken in DTE3 in preparation for ITER's nuclear operation, which were not considered in DTE2 [100]. In DTE3, an experiment to assess the activation of cooling water was performed for the first time. Water circulating in the cooling pipes is activated by high-energy neutrons and then transported through the cooling circuits. This induces additional heat loads and an increased radiation dose to the machine components. Sensitive systems outside the bioshield may also receive significant radiation doses [104]. The first measurements of water activation in a real tokamak cooling loop during D-T operation were obtained in the cooling loop of the NBI system in Octant 4 (at the NBI duct scraper). Once calibration is complete, the measured activation level will be compared against the anticipated peak value of the order of $3 \cdot 10^7$ Bq, estimated in advance under conservative assumptions [105] and will allow the validation of predictions made for water activation in ITER [105, 106]. Another major concern for ITER is the potential for neutron-induced failures

in electronic systems. To complement studies at WEST in D operations [107] and CERN dedicated test benches and measurement systems were installed in the JET basement to measure Single Event Effects on electronics (caused by instantaneous interaction of a single neutron with the material) for the first time in D-T operations. This unprecedented systematic study of such effects in a real tokamak environment confirmed the modeling and predictions of Single Event Effect under D-T operations [108].

10. Addressing outstanding issues from the DTE2 campaign

Part of the DTE3 campaign was devoted to addressing the open questions remaining from the T and DTE2 campaigns [10], in order to complete and consolidate the work done in these campaigns by extending the physics understanding of the topics addressed. As noted in section 2, it was not deemed advantageous to attempt to increase the fusion performance beyond the DTE2 achievements, and this was not part of the objectives of the DTE3 scientific program. The main topics are briefly described below.

10.1. Studies on RF heating schemes

The second harmonic ICRF heating of tritium $2\omega_c(\mathrm{T})$ was shown to be capable of providing bulk ion heating in ITER-relevant conditions in DTE2 [109], increasing the confidence in this reference ICRF scheme for ITER D-T plasmas at a magnetic field of 5.3 T. In DTE3, as only deuterium NBI was available and fast T was not present, experiments could be carried out to investigate the role of the ICRF-NBI synergy in D-T plasmas ($n_\mathrm{D} \sim n_\mathrm{T}$) [110], with a small amount of ^{3}He intrinsically in the plasma (0.2%–0.4%). The studies were performed, as in DTE2, with H-mode pulses at 3.4 T, 2.2 MA, with $P_\mathrm{RF} \sim 2{-}4.5$ MW (central resonance) and $P_\mathrm{NBI} = 22 - 29$ MW. However, the differences observed between the DTE2 pulses (with D- and T-NBI) and the DTE3 pulses (only D-NBI) could not be explained by the differences in heating [111] given that the bulk ion heating reduced by ∼7% and the bulk electron heating was increased by ∼33%, when only D-NBI was used (with respect to the pulses with D- and T-NBI). A decrease in the ion to electron temperature ratio would have been expected, while both the ion and electron temperature decreased at fixed $T_\mathrm{i}/T_\mathrm{e}$. Additional effects need to be considered to explain the observations, such as transport, fast particles, impurities, MHD or machine conditions. The RF scheme based on $\omega = \omega_c(^3\mathrm{He}) = 2\omega_c(\mathrm{T})$ was also compared in L-modes with the more commonly used scheme on $\omega = \omega_c(\mathrm{H})$ and was found to perform equally well [111].

The three-ion RF heating scenarios [112] were also further investigated in DTE3. A novel ITER-relevant ICRF scheme, which can heat D-T plasmas with $n_\mathrm{D} \sim n_\mathrm{T}$ using ^{9}Be impurities inherent in JET plasmas with the Be/W wall, was demonstrated in DTE2 and was shown to efficiently heat the core plasma locally with a significant increase in the core ion temperature [113]. In DTE3, the three-ion RF scheme heating ^{9}Be impurities ($f_\mathrm{RF} = 25$ MHz, $\mathrm{B_T} = 3.7$ T) was compared with the RF scheme heating H minority ions ($f_\mathrm{RF} = 55$ MHz, $\mathrm{B_T} = 3.7$ T) in D-T plasmas. A higher core ion temperature was observed with the three-ion scheme (predominantly ion heating, T_i increasing from ~ 3.0 keV to ~ 5.5 keV), while a higher core electron temperature was observed with the H-minority scheme (predominantly electron heating, T_e increasing from ~ 3.5 keV to ~ 6.5 keV), when 2.5 MW of ICRF power was added to the L-mode D-T plasmas ($n_\mathrm{D} \sim n_\mathrm{T}$, 3.7 T, 2.0 MA), pre-heated with 7.5 MW of NBI [114]. In addition, a three-ion RF scheme heating argon impurities was tested. The increase of T_i with ICRF was experimentally observed with argon levels up to $\sim 0.1\%$.

The fundamental ($n = 1$) harmonic ICRF heating of D was also investigated. In ITER, the bulk D ions will efficiently absorb the majority of the ICRF power at the fundamental D frequency in plasmas with $n_\mathrm{D} \sim n_\mathrm{T}$ (40 MHz at 5.3 T) [115]. This scheme was expected to work also in JET plasmas with $n_\mathrm{D} \sim n_\mathrm{T}$ [116, 117]. It was now tested in DTE3 and was demonstrated to have similar power absorption efficiency as in the T-rich case, with significant fraction of the power absorbed by ions [118].

Finally, the new DTE3 experiments will contribute further to the understanding of the interaction between RF waves and fusion-born α-particles. DTE2 experiments had found that energetic α-particles have sufficient energy to interact effectively with RF waves, with moderate changes in their distribution predicted and observed experimentally, but with negligible impact on their losses and the electron and ion heating they provide [119].

10.2. Dependence of heat and particle transport and L-H power threshold on the isotope mass

One of the main objectives of the T and DTE2 campaigns was the characterisation of the heat and particle transport in type-I ELMy H-mode plasmas containing tritium. Despite the extensive experimental investigations and modelling activities, which provided crucial information for understanding the isotope dependence in the plasma core and the pedestal [47], some questions remained open that could be addressed experimentally. Experiments were performed to assess the pedestal of T-rich and D-T plasmas at higher gas fuelling than previously investigated. The ongoing analysis aims to clarify whether the pedestal of a D-T plasma degrades with gas fuelling, similar to what is observed in H or D plasmas, or whether it is constant as in T plasmas, and whether the pedestal of T-rich plasmas degrades at even higher gas fuelling.

The T and DTE2 campaigns also addressed the L-H power threshold in T, D-T and H-T plasmas to complement the thorough investigation in H and D plasmas [120]. In DTE3, information on the L-H power threshold in the low and high density range, which was missing from the previous investigations, was obtained. Furthermore, a controller to tailor the H-mode entry was developed, via monitoring the ratio of the power across the separatrix over the L-H power threshold and

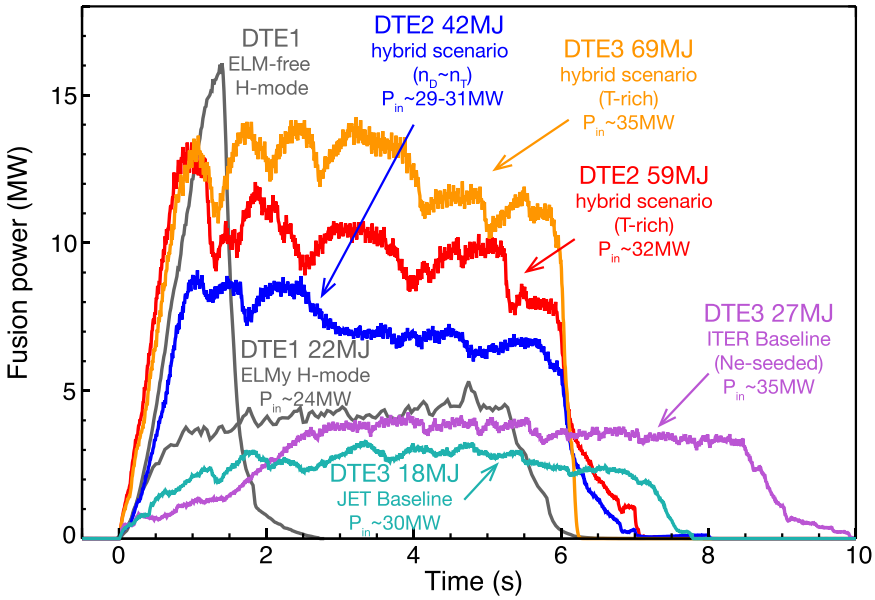

Figure 7. Fusion power produced in JET in DTE1 (ELM-free H-mode #42976 and ELMy H-mode #42982, in grey), DTE2 (hybrid scenario with $n_D \sim n_T$ #99869 in blue, T-rich hybrid scenario #99971 in red) and DTE3 campaigns (T-rich hybrid scenario #104522 in orange, Ne-seeded ITER baseline scenario #104600 in purple, JET baseline scenario #104663 in teal).

using the NBI power and the fuelling as actuators, and was successfully tested in DTE3 [121].

10.3. Scenarios for high, sustained fusion power

The JET hybrid scenario achieved sustained high fusion power production in DTE2, reaching record values of fusion energy in a D-T plasma with $n_D \sim n_T$ (46 MJ) [57]. One of the open questions following the DTE2 experiments concerned a possible isotope effect on the formation of the internal transport barrier (ITB) observed in hybrid plasmas in D but not in D-T. In dedicated experiments to study the ITB formation in D-T, it was observed that a similar ITB could be observed on the ion temperature profile in D-T plasmas with a T-rich ohmic current ramp (similar to that described in section 5), as in the comparison D plasmas. Preliminary evidence suggests that the isotope effects do not play a major role, but rather an early gas puff prevented the development of a strong ITB.

The JET baseline scenario was not successfully sustained long enough in DTE2, although the plasmas were stable for 5 s in D [10, 30]. The scenario was revisited in DTE3 to understand the physics reasons why it was not possible to sustain the plasmas at the envisaged plasma current of 3.5 MA. Neither sufficient input power, nor sufficient experimental time was available to develop the scenario at 3.0 MA in DTE2. Experiments at 3.5 MA were not performed as this was considered to be a high risk for the machine (a potential leak would have compromised the plasma facing component samples, which will be removed from the vessel for further analysis). MHD activity limited the plasma performance when the maximum available input power was used (at 3.0 MA, 2.9 T). This was successfully mitigated by slightly reducing the input power ($P_{NBI} \sim 27$ MW, $P_{RF} \sim 3$ MW), and for the first time a JET baseline pulse could be sustained in D-T for 5 s in DTE3, until the programmed pulse termination, albeit with a slight decrease in the neutron rate [122]. The fusion power produced in this pulse #104663 can be seen in figure 7. No time was available to optimise the pulse further. These data complement the DTE2 pulses and are now being analysed to understand the difficulties in establishing baseline scenario plasmas at high plasma current, and publications are in preparation. Specifically, the JET baseline scenario's inability to achieve a stationary pulse in D-T has been attributed to the fact that the fuelling scheme has not been able to sustain the necessary ELM activity. This scheme, which was successful in D in maintaining a stable density and radiated power, did not translate to D-T operations. The reader is reminded that this scenario does not use impurity seeding and is different from the one described in section 3, among others with regard to the plasma shape and the divertor configuration.

10.4. Increasing the stationarity of the T-rich hybrid scenario

Tritium-rich hybrid scenario pulses delivered a fusion energy record of 59 MJ in DTE2, a world fusion energy record at the time [17]. This success was made possible by optimising the plasma composition and heating methods. Deuterium NBI was used to heat a tritium-rich plasma to maximise non-thermal fusion reactions, and RF heating was applied at the fundamental harmonic ($n = 1$) D resonance which further increased the D-T fusion power due to the enhanced acceleration of deuterium by the applied RF power [117]. The plasma scenario relied on the fast isotope transport (mixing) effect to keep the deuterium-tritium ratio under control [123, 124]. This scenario was revisited in DTE3 in an attempt to improve the pulse stationarity. With higher P_{RF} (from ~ 3.8 MW to ~ 5.5 MW), the plasma was shown to be more resilient to high-Z impurity

accumulation. The reproducibility of this plasma scenario was confirmed.

As a result, a new fusion energy world record of 69 MJ was achieved. Figure 7 shows the fusion power produced in JET in all three D-T campaigns with a substantial tritium concentration. For DTE1, the ELM-free H-mode pulse that transiently produced very high fusion power (>15 MW) and an ELMy H-mode pulse with stationary fusion power production are shown in grey. Two hybrid scenario pulses performed in DTE2, one with $n_{\mathrm{D}} \sim n_{\mathrm{T}}$ and one T-rich ($n_{\mathrm{T}}/(n_{\mathrm{D}}+n_{\mathrm{T}}) \sim 0.85$) are shown in blue and red, respectively. The T-rich hybrid scenario pulse, which produced the latest fusion energy world record obtained in DTE3 is shown in orange. A Ne-seeded ITER baseline scenario pulse from DTE3, the only one in this set with a high radiation fraction due to a seeding impurity and a partially detached divertor, is shown in purple.

11. Summary and outlook

The third and last D-T campaign with a substantial tritium concentration at JET in 2023 successfully complemented the deuterium experiments in 2022–2023 [12]. The focus was on the development of scenarios for ITER and DEMO, the extension of the physics understanding and prediction capabilities for future devices. The DTE3 campaign was based on the scientific objectives and experiments of the previous deuterium campaigns. These deuterium campaigns included the development of a radiative high current scenario for ITER and the transfer of plasma regimes developed in medium-size tokamaks to JET (such as the QCE and XPR regimes). Several other topics were investigated in D, such as strategies for disruption and runaway mitigation and high-beta long-pulse scenarios, which were not included in DTE3 and are therefore not addressed in this publication [12]. The extensive effort devoted to the development of the different plasma scenarios in D has made it possible to demonstrate the scenarios in D-T in a straightforward manner and to assess the changes with the different isotope masses. The lessons learned during the T and DTE2 campaigns [14] and their implementation were crucial for the efficient execution and successful results of the DTE3 campaign. It was made clear that the recent experience, both technical and scientific, with D-T plasmas and nuclear operations was extremely beneficial, a point that should be considered with a view towards future nuclear fusion devices, as discussed in section 2 [14].

The scientific objectives of the DTE3 campaign, introduced in section 2, have been successfully addressed, and the key results are summarized below. This also highlights the next steps in analysis and modelling that are necessary to inform ITER and future fusion devices:

(i) In view of ITER, a core-edge-SOL integrated H-mode scenario has been developed and tested in D-T in support of ITER [31, 32, 35] (section 3). This scenario operates in an ITER-like plasma shape configuration, shows good confinement and the divertor is partially detached with the use of Ne-seeding. D-T operations extended the scenario parameter space, as only in D-T high performance with Ne-seeding was possible at 3.0 MA, and highlighted the impact of the higher isotope mass. Stationary pulses with good performance, no tungsten accumulation and even without ELMs were achieved in D-T. An extensive data set is now available in both D and D-T to benchmark of core, edge and core-edge integrated modelling codes and to provide valuable information for ITER. An additional challenge for the integrated modelling used to provide predictions for ITER based on these results will be to account for the recent change in the planned wall material for ITER, from Be/W to all-W [125]. Several aspects are being investigated, relating to the impact of the radiating seeded impurity on the plasma confinement, the pedestal and SOL characteristics, the partial detachment access criteria, the source and transport of tungsten, and the underlying mechanisms for the suppression of type-I ELMs.

(ii) Plasmas with a pedestal limited by peeling modes, such as may be encountered in ITER, have also been studied with D, T-rich and D-T fuel [44, 45] (section 4). For all isotopes, a positive correlation between pedestal electron pressure and pedestal electron density was observed, in contrast to the case of ballooning-limited pedestals. The pedestal pressure does not decrease with increasing $n_{\mathrm{e}^{\mathrm{sep}}}/n_{\mathrm{e}^{\mathrm{ped}}}$. The peeling-limited pedestals characteristics and the impact of the isotope mass are currently being compared in detail with ballooning-limited pedestals, as well as with peeling-limited pedestals achieved in smaller devices.

(iii) The conditions of impurity (tungsten) screening at the plasma periphery, as predicted for ITER, have been further explored in hybrid scenario plasmas [59, 60] (section 5). Scenario adjustments have improved the diagnostic coverage in D-T, which was lacking in previous studies [57]. Detailed transport modelling is now underway to understand the physics mechanisms behind the experimental observations of tungsten screening.

(iv) In view of DEMO, a scenario without type-I ELMs, the QCE regime, was successfully achieved with D-T fuel [73, 74] (section 6). The access criteria for strong shaping and high separatrix density are similar in D-T [72]. The QCE follows the expectations of higher pressure in D-T with respect to D plasmas. The details of the pedestal changes from D to D-T, namely the increase of the temperature and not only the density, remain to be understood.

(v) The X-point radiator regime, a scenario with full detachment as required for DEMO, was established in D-T, aided by the real-time control of the XPR position previously developed in D plasmas [78] (section 7). A mixture of argon and neon was found to be the best seeding candidate, as in D plasmas, and the changes in plasma performance from D to D-T were in line with expectations. SOL and divertor modeling is now

underway to improve the understanding of the XPR also across isotopes and to enable predictions for ITER and DEMO.

(vi) The characterisation of tritium retention continued in DTE3, using gas balance measurements for global fuel retention measurements and the new LID-QMS diagnostic for local in-situ fuel retention measurements [88, 89] (section 8). Preliminary results show that fuel retention is independent of the fuel mass. The LID-QMS provided the first in-situ tritium measurements, which were shown to be in qualitative agreement with the predictions. As after DTE2, tritium clean-up operations were carried out after DTE3, and information on the effectiveness of different methods was collected. The data obtained before, during and after DTE3 require comprehensive analysis to draw conclusions on the tritium retention and clean-up, and will provide valuable information for ITER and all future fusion devices. The work will continue with in-situ LIBS measurements now that the JET vessel has been vented, and will be completed after the analysis of the plasma-facing-component samples that will be removed in the future.

(vii) In preparation for ITER's nuclear operation, nuclear technology studies were advanced during the DTE3 campaign (section 9), with two issues being addressed for the first time in a tokamak environment under D-T operations, namely the activation of water in cooling loops and single event effects on electronics [100, 103].

(viii) Several outstanding issues from the DTE2 campaign were revisited in DTE3. These included the characterisation of RF schemes [111, 114] (section 10.1), and the impact of isotope mass on the L-H power threshold [120] and on the heat and particle transport [47] (section 10.2). The impact of the isotope mass on the formation of the ITB in the JET hybrid scenario [57] was evaluated and excluded. The JET baseline scenario [10, 30] achieved a stationary pulse in D-T for the first time, shedding light on the causes why this was previously not achieved (section 10.3). Efforts to increase the stationarity of the T-rich hybrid scenario [17] led to a further fusion energy world record of 69 MJ (section 10.4).

Further to these objectives, real-time control schemes relevant to D-T operations have been developed. In addition to the real-time control of the X-point radiator position, developed in D and also demonstrated in DTE3, the control of the D-T plasma fuel mixture was successfully demonstrated in DTE3 [126, 127]. As in DTE2, 'dud' detectors were used to detect pulses that are not performing as well as expected and to trigger an appropriate termination sequence, allowing the efficient use of both the tritium and the neutron budgets [128, 129].

The analysis of the wealth of data collected during the recent JET experimental campaigns in D and D-T is underway. Interpretative modelling will address the open questions and allow the comparison of D and D-T plasmas. In many cases, the data will be used to validate the modelling codes. Predictive modelling will then be used to extrapolate to ITER and DEMO. These experiments offer a unique opportunity to validate and refine the models that underpin ITER's performance expectations, based on the physics understanding. JET was shut down at the end of 2023, after 40 years of unique contributions to fusion research [1]. The DTE3 campaign at JET added to the valuable lessons learned from previous T and D-T operations at JET, providing experience and understanding not only for ITER and DEMO, but for any magnetic confinement fusion device using D-T fuel.

Data availability statement

Overview of wider range of experiments that is based on more dedicated and specialised publications (partially to come). The data that support the findings of this study are available upon reasonable request from the authors.

Acknowledgments

The authors acknowledge and thank the JET team for their hard work and commitment. This work has been carried out within the framework of the EUROfusion Consortium, funded by the European Union via the Euratom Research and Training Programme (Grant Agreement No 10 105 2200 - EUROfusion). The Swiss contribution to this work has been funded by the Swiss State Secretariat for Education, Research and Innovation (SERI). This work was supported in part by Grant PID2021-12 7727OB-I00, funded by the Spanish Ministry of Science, Innovation and Universities MICIU/AEI/10.13 039/50 110 0011 033, and by ERDF/EU. This scientific paper has been published as part of the international project co-financed by the Polish Ministry of Science and Higher Education within the programme called 'PMW' for 2022–2024. Views and opinions expressed are however those of the author(s) only and do not necessarily reflect those of the European Union, the European Commission or SERI. Neither the European Union nor the European Commission nor SERI can be held responsible for them.

ORCID iDs

A Kappatou https://orcid.org/0000-0003-3341-1909
M Baruzzo https://orcid.org/0009-0006-7853-7280
A Hakola https://orcid.org/0000-0003-1385-1296
E Joffrin https://orcid.org/0009-0008-7527-0984
D Keeling https://orcid.org/0000-0002-3581-7788
B Labit https://orcid.org/0000-0002-0751-8182
N Vianello https://orcid.org/0000-0003-4401-5346
M Wischmeier https://orcid.org/0000-0002-3065-027X
I Balboa https://orcid.org/0000-0002-5665-2222
J Bernardo https://orcid.org/0000-0002-8197-7432
M Bernert https://orcid.org/0000-0003-1131-0867
T Bosman https://orcid.org/0000-0002-7922-7974
S Brezinsek https://orcid.org/0000-0002-7213-3326
D Brida https://orcid.org/0000-0002-8647-7058
I S Carvalho https://orcid.org/0000-0002-2458-8377

P Carvalho https://orcid.org/0000-0002-8480-0499
L Ceelen https://orcid.org/0000-0002-6574-1841
I Coffey https://orcid.org/0009-0006-6055-6045
T Dittmar https://orcid.org/0000-0002-4325-7979
M Dunne https://orcid.org/0000-0002-5259-9970
M Faitsch https://orcid.org/0000-0002-9809-7490
A R Field https://orcid.org/0000-0003-0671-9668
L Frassinetti https://orcid.org/0000-0002-9546-4494
L Garzotti https://orcid.org/0000-0002-3796-9814
S Henderson https://orcid.org/0000-0002-8886-1256
R B Henriques https://orcid.org/0000-0003-0585-0904
J Hobirk https://orcid.org/0000-0001-6605-0068
P Jacquet https://orcid.org/0009-0007-9916-2032
I Jepu https://orcid.org/0000-0001-8567-3228
Ye O Kazakov https://orcid.org/0000-0001-6316-5441
D B King https://orcid.org/0000-0001-5128-5083
K K Kirov https://orcid.org/0000-0001-8104-4782
D Kos https://orcid.org/0000-0002-9550-4329
K Krieger https://orcid.org/0000-0003-0427-8184
M Lennholm https://orcid.org/0000-0002-3444-3999
E Lerche https://orcid.org/0000-0003-4584-3581
X Litaudon https://orcid.org/0000-0001-6973-9717
E Litherland-Smith https://orcid.org/0009-0000-0587-2930
J Mailloux https://orcid.org/0009-0005-4265-5480
M J Mantsinen https://orcid.org/0000-0001-9927-835X
M Maslov https://orcid.org/0000-0001-8392-4644
D Matveev https://orcid.org/0000-0001-6129-8427
A Meigs https://orcid.org/0000-0002-8071-864X
S Menmuir https://orcid.org/0000-0003-3250-0256
C Perez von Thun https://orcid.org/0000-0002-1166-2179
L Piron https://orcid.org/0000-0002-7928-4661
G Pucella https://orcid.org/0000-0002-9923-2770
H Reimerdes https://orcid.org/0000-0002-9726-1519
F Rimini https://orcid.org/0009-0001-2917-0455
O Sauter https://orcid.org/0000-0002-0099-6675
P A Schneider https://orcid.org/0000-0001-7257-3412
B Sieglin https://orcid.org/0000-0002-9480-4434
S Silburn https://orcid.org/0000-0002-3111-5113
E R Solano https://orcid.org/0000-0002-4815-3407
H Sun https://orcid.org/0000-0003-0880-0013
D F Valcarcel https://orcid.org/0000-0002-5573-2095
D van Eester https://orcid.org/0000-0002-4284-3992
R Villari https://orcid.org/0000-0001-7972-1676
A Widdowson https://orcid.org/0000-0002-6805-8853
S Wiesen https://orcid.org/0000-0002-3696-5475
M Zlobinski https://orcid.org/0000-0002-1395-7165
V K Zotta https://orcid.org/0000-0002-3518-5178

References

[1] Rimini F *et al* 2025 40 years of JET operations: a unique contribution to fusion science *Plasma Phys. Control. Fusion* **67** 033001
[2] Strachan J D *et al* 1997 TFTR DT experiments *Plasma Phys. Control. Fusion* **39** B103
[3] Hawryluk R J 1998 Results from deuterium-tritium tokamak confinement experiments *Rev. Mod. Phys.* **70** 537–87
[4] G H Neilson ed 2016 *Magnetic Fusion Energy : From Experiments to Power Plants*
[5] Joffrin E *et al* 2019 Overview of the JET preparation for deuterium-tritium operation with the ITER like-wall *Nucl. Fusion* **59** 112021
[6] JET Team 1992 Fusion energy production from a deuterium-tritium plasma in the JET tokamak *Nucl. Fusion* **32** 187
[7] Jacquinot J *et al* 1999 Overview of ITER physics deuterium-tritium experiments in JET *Nucl. Fusion* **39** 235
[8] Keilhacker M *et al* 1999 High fusion performance from deuterium-tritium plasmas in JET *Nucl. Fusion* **39** 209
[9] Matthews G F *et al* 2011 JET ITER-like wall-overview and experimental programme *Phys. Scr.* **2011** 014001
[10] Maggi C (JET Contributors) 2024 Overview of T and D-T results in JET with ITER-like wall *Nucl. Fusion* **64** 112012
[11] 2019 European research roadmap to the realisation of fusion energy *Technical Report* EUROfusion
[12] Joffrin E *et al* 2024 Overview of the EUROfusion tokamak exploitation programme in support of ITER and DEMO *Nucl. Fusion* **64** 112019
[13] Mailloux J *et al* 2022 Overview of JET results for optimising ITER operation *Nucl. Fusion* **62** 042026
[14] The JET Operations Team (presented by D.B. King) 2024 JET machine operations in T and D-T *Nucl. Fusion* **64** 106014
[15] King D B *et al* 2022 Tritium operation of the JET neutral beam systems and tritium NBI power calculations *IEEE Trans. Plasma Sci.* **50** 4080–5
[16] King D B *et al* 2023 Tritium neutral beam injection on JET: calibration and plasma measurements of stored energy *Nucl. Fusion* **63** 112005
[17] Maslov M *et al* 2023 JET D-T scenario with optimized non-thermal fusion *Nucl. Fusion* **63** 112002
[18] Bell A, Ballantyne P, Gordont C and Wright M 1999 The safety case for JET D-T operation *Fusion Eng. Des.* **47** 115–30
[19] Boyer H, Plummer D and Johnston J 2016 JET tokamak, preparation of a safety case for tritium operations *Fusion Eng. Des.* **109–111** 1308–12
[20] Bickerton S *et al* 2023 Operational and engineering experiences of gas injection to JET for TT and DT operational campaigns *Plasma Phys. Control. Fusion* **65** 094001
[21] Carvalho I S *et al* 2017 Operational aspects of the JET tritium introduction modules *Fusion Eng. Des.* **124** 841–5
[22] Felton R *et al* 2024 Operational aspects of tritium injection into the JET tokamak *Plasma Phys. Control. Fusion* submitted
[23] Shimada M *et al* 2007 Chapter 1: overview and summary *Nucl. Fusion* **47** S1
[24] Sips A C C *et al* 2018 Assessment of the baseline scenario at q95~3 for ITER *Nucl. Fusion* **58** 126010
[25] 2024 ITER Research Plan within the Staged Approach *Technical Report* ITR-24-005 ITER Organisation
[26] Pitts R A *et al* 2019 Physics basis for the first ITER tungsten divertor *Nucl. Mater. Energy* **20** 100696
[27] Drenik A *et al* 2019 Evolution of nitrogen concentration and ammonia production in N2-seeded H-mode discharges at ASDEX Upgrade *Nucl. Fusion* **59** 046010
[28] Giroud C *et al* 2021 High performance ITER-baseline discharges in deuterium with nitrogen and neon-seeding in the JET-ILW *28th IAEA Fusion Energy Conf. (Virtual Event, 10 May–15 May 2021)* [EX/3-9]
[29] Giroud C *et al* 2024 The core-edge integrated neon-seeded scenario in deuterium-tritium at JET *Nucl. Fusion* **64** 106062
[30] Garzotti L *et al* 2023 Development of high current baseline scenario for high deuterium-tritium fusion performance at

JET *29th IAEA Fusion Energy Conf. (London, 16 October–21 October 2023)* [EX/7–3]
[31] Giroud C *et al* 2024 High-current neon-seeded ITER baseline scenario in JET D and D-T *26th Int. Conf. on Plasma Surface Interaction* (*Marseille, France*)
[32] Giroud C *et al* 2025 *Nucl. Fusion* (in preparation)
[33] Carvalho I S *et al* 2025 *Nucl. Fusion* (in preparation)
[34] Sauter O, Angioni C and Lin-Liu Y R 1999 Neoclassical conductivity and bootstrap current formulas for general axisymmetric equilibria and arbitrary collisionality regime *Phys. Plasmas* **6** 2834–9
[35] Carvalho I S *et al* 2024 Neon seeded ITER baseline scenario experiments in JET D and D-T plasmas *50th EPS Conf. on Plasma Physics* (*Salamanca, Spain*)
[36] Verdoolaege G *et al* 2021 The updated ITPA global H-mode confinement database: description and analysis *Nucl. Fusion* **61** 076006
[37] Eriksson F *et al* 2024 Simulations of the stationary Q = 10 and the exit phase from the flat-top of an ITER 15MA baseline scenario: predictive JINTRAC simulation with a consistent treatment of D and T in the whole plasma *Nucl. Fusion* **64** 126033
[38] Matthews G F *et al* 2017 Dynamic power balance analysis in JET *Phys. Scr.* **2017** 014035
[39] Saarelma S *et al* 2012 Edge stability analysis of ITER baseline plasma simulations *Nucl. Fusion* **52** 103020
[40] Snyder P B *et al* 2015 Super H-mode: theoretical prediction and initial observations of a new high performance regime for tokamak operation *Nucl. Fusion* **55** 083026
[41] Frassinetti L *et al* 2022 Pedestal structure and stability near the peeling boundary in TCV *48th EPS Conf. on Plasma Physics* (*online*)
[42] Dunne M G *et al* 2016 Global performance enhancements via pedestal optimisation on ASDEX Upgrade *Plasma Phys. Control. Fusion* **59** 025010
[43] Frassinetti L *et al* 2020 Pedestal structure, stability and scalings in JET-ILW: the EUROfusion JET-ILW pedestal database *Nucl. Fusion* **61** 016001
[44] Frassinetti L *et al* 2024 Peeling limited pedestal experiments in JET-ILW and MAST-U *50th EPS Conf. on Plasma Physics* (*Salamanca, Spain*)
[45] Frassinetti L *et al* 2024 Low collisionality, peeling limited pedestals in JET-ILW: effect of density and isotope mass on pedestal structure, pedestal stability and pedestal prediction in deuterium and mixed deuterium/tritium plasmas *Nucl. Fusion* submitted
[46] Frassinetti L *et al* 2023 Effect of the isotope mass on pedestal structure, transport and stability in D, D/T and T plasmas at similar βN and gas rate in JET-ILW type I ELMy H-modes *Nucl. Fusion* **63** 112009
[47] Schneider P A *et al* 2023 Isotope physics of heat and particle transport with tritium in JET-ILW type-I ELMy H-mode plasmas *Nucl. Fusion* **63** 112010
[48] Saarelma S *et al* 2019 Self-consistent pedestal prediction for JET-ILW in preparation of the DT campaign *Phys. Plasmas* **26** 072501
[49] Frassinetti L *et al* 2019 Role of the pedestal position on the pedestal performance in AUG, JET-ILW and TCV and implications for ITER *Nucl. Fusion* **59** 076038
[50] Wilks T M *et al* 2021 Development of an integrated core-edge scenario using the super H-mode *Nucl. Fusion* **61** 126064
[51] Pütterich T *et al* 2019 Determination of the tolerable impurity concentrations in a fusion reactor using a consistent set of cooling factors *Nucl. Fusion* **59** 056013
[52] Hirshman S and Sigmar D 1981 Neoclassical transport of impurities in tokamak plasmas *Nucl. Fusion* **21** 1079
[53] Angioni C 2021 Impurity transport in tokamak plasmas, theory, modelling and comparison with experiments *Plasma Phys. Control. Fusion* **63** 073001
[54] Dux R, Loarte A, Fable E and Kukushkin A 2014 Transport of tungsten in the H-mode edge transport barrier of ITER *Plasma Phys. Control. Fusion* **56** 124003
[55] Dux R *et al* 2017 The interplay of controlling the power exhaust and the tungsten content in ITER *Nucl. Mater. Energy* **12** 28–35
[56] Field A R *et al* 2022 Peripheral temperature gradient screening of high-Z impurities in optimised 'hybrid' scenario H-mode plasmas in JET-ILW *Nucl. Fusion* **63** 016028
[57] Hobirk J *et al* 2023 The JET hybrid scenario in Deuterium, Tritium and Deuterium-Tritium *Nucl. Fusion* **63** 112001
[58] Fajardo D *et al* 2023 Analytical model for the combined effects of rotation and collisionality on neoclassical impurity transport *Plasma Phys. Control. Fusion* **65** 035021
[59] King D B *et al* 2025 Development of JET Hybrid Plasmas in Deuterium and Deuterium-Tritium for Impurity Screening *Plasma Phys. Control. Fusion* (in preparation)
[60] Olde C *et al* 2024 Impurity screening in hybrid scenario plasmas in JET-ILW *66th Annual Meeting of the APS Division of Plasma Physics* (Atlanta, GA)
[61] Field A R *et al* 2025 Optimisation of 'hybrid' scenario H-mode plasmas for W radiation control in JET-ILW *Nucl. Fusion* (in preparation)
[62] Fajardo D, Angioni C, Maget P and Manas P 2022 Analytical model for collisional impurity transport in tokamaks at arbitrary collisionality *Plasma Phys. Control. Fusion* **64** 055017
[63] Belli E A and Candy J 2008 Kinetic calculation of neoclassical transport including self-consistent electron and impurity dynamics *Plasma Phys. Control. Fusion* **50** 095010
[64] Belli E A and Candy J 2009 An Eulerian method for the solution of the multi-species drift-kinetic equation *Plasma Phys. Control. Fusion* **51** 075018
[65] Belli E A and Candy J 2011 Full linearized Fokker-Planck collisions in neoclassical transport simulations *Plasma Phys. Control. Fusion* **54** 015015
[66] Faitsch M *et al* 2021 Broadening of the power fall-off length in a high density, high confinement H-mode regime in ASDEX Upgrade *Nucl. Mater. Energy* **26** 100890
[67] Harrer G F *et al* 2022 Quasicontinuous exhaust scenario for a fusion reactor: The renaissance of small edge localized modes *Phys. Rev. Lett.* **129** 165001
[68] Labit B (the MST1 Team) 2019 Dependence on plasma shape and plasma fueling for small edge-localized mode regimes in TCV and ASDEX Upgrade *Nucl. Fusion* **59** 086020
[69] Faitsch M *et al* 2023 Analysis and expansion of the quasi-continuous exhaust (QCE) regime in ASDEX Upgrade *Nucl. Fusion* **63** 076013
[70] Radovanovic L *et al* 2022 Developing a physics understanding of the quasi-continuous exhaust regime: pedestal profile and ballooning stability analysis *Nucl. Fusion* **62** 086004
[71] Eich T and Manz P (the ASDEX Upgrade team) 2021 The separatrix operational space of ASDEX Upgrade due to interchange-drift-Alfvén turbulence *Nucl. Fusion* **61** 086017
[72] Dunne M *et al* 2024 Quasi-continuous exhaust operational space *Nucl. Fusion* **64** 124003
[73] Faitsch M *et al* 2025 The quasi-continuous exhaust regime in ASDEX Upgrade and JET *Nucl. Mater. Energy* **42** 101904
[74] Faitsch M *et al* 2025 The quasi-continuous exhaust regime in JET *Nucl. Fusion* **65** 024003

[75] Saibene G *et al* 2005 Characterization of small ELM experiments in highly shaped single null and quasi-double-null plasmas in JET *Nucl. Fusion* **45** 297

[76] Wischmeier M 2015 High density operation for reactor-relevant power exhaust *J. Nucl. Mater.* **463** 22–29

[77] Bernert M *et al* 2017 Power exhaust by SOL and pedestal radiation at ASDEX Upgrade and JET *Nucl. Mater. Energy* **12** 111–8

[78] Bernert M *et al* 2025 X-point radiation: from discovery to potential application in a future reactor *Nucl. Mater. Energy* **43** 101916

[79] Stroth U *et al* 2022 Model for access and stability of the X-point radiator and the threshold for marfes in tokamak plasmas *Nucl. Fusion* **62** 076008

[80] Bernert M *et al* 2020 X-point radiation, its control and an ELM suppressed radiating regime at the ASDEX Upgrade tokamak *Nucl. Fusion* **61** 024001

[81] Sieglin B *et al* 2023 Disruption avoidance and investigation of the H-Mode density limit in ASDEX Upgrade *Plasma Phys. Control. Fusion* **66** 025004

[82] Bosman T *et al* 2024 X-point radiator control and its dynamics in ASDEX Upgrade and JET deuterium-tritium discharges *Nucl. Fusion* **65** 016057

[83] Glöggler S *et al* 2019 Characterisation of highly radiating neon seeded plasmas in JET-ILW *Nucl. Fusion* **59** 126031

[84] Andrew P *et al* 1999 Tritium retention and clean-up in JET *Fusion Eng. Des.* **47** 233–45

[85] Peacock A T *et al* 2000 Tritium inventory in the first wall of JET *Fusion Eng. Des.* **49–50** 745–52

[86] Brezinsek S *et al* 2013 Fuel retention studies with the ITER-Like Wall in JET *Nucl. Fusion* **53** 083023

[87] Widdowson A *et al* 2014 Material migration patterns and overview of first surface analysis of the JET ITER-like wall *Phys. Scr.* **2014** 014010

[88] Widdowson A *et al* 2024 Overview of fuel retention and recovery in JET deuterium-tritium operation *Nucl. Fusion* submitted

[89] Widdowson A *et al* 2024 Overview of fuel retention and recovery in JET DT operation *26th Int. Conf. on Plasma Surface Interaction* (*Marseille, France*)

[90] Widdowson A *et al* 2021 Evaluation of tritium retention in plasma facing components during JET tritium operations *Phys. Scr.* **96** 124075

[91] Matveev D *et al* 2023 Tritium removal from JET-ILW after T and D-T experimental campaigns *Nucl. Fusion* **63** 112014

[92] Loarer T 2009 Fuel retention in tokamaks *J. Nucl. Mater.* **390–391** 20–28

[93] Zlobinski M *et al* 2024 First results of laser-induced desorption - quadrupole mass spectrometry (LID-QMS) at JET *Nucl. Fusion* **64** 086031

[94] Heinola K *et al* 2017 Experience on divertor fuel retention after two ITER-like wall campaigns *Phys. Scr.* **2017** 014063

[95] LaGuardia L *et al* 2024 JET residual gas analyzer calibrations during LID-QMS operations *26th Int. Conf. on Plasma Surface Interaction* (*Marseille, France*)

[96] Semerok A *et al* 2016 Laser induced breakdown spectroscopy application in Joint European Torus *Spectrochim. Acta* B **123** 121–8

[97] Likonen J *et al* 2014 First results and surface analysis strategy for plasma-facing components after JET operation with the ITER-like wall *Phys. Scr.* **2014** 014016

[98] Krat S *et al* 2020 Comparison of erosion and deposition in JET divertor during the first three ITER-like wall campaigns *Phys. Scr.* **2020** 014059

[99] Wauters T *et al* 2022 Isotope removal experiment in JET-ILW in view of T-removal after the 2nd DT campaign at JET *Phys. Scr.* **97** 044001

[100] Villari R *et al* 2024 Overview of deuterium-tritium nuclear operations at JET *33rd Symp. on Fusion Technology (SOFT2024)* (*Dublin, Ireland*)

[101] Villari R *et al* 2023 Technological aspects of recent D-T operations at JET *15th Int. Symp. on Fusion Nuclear Technology* (*Gran Canaria, Spain*)

[102] Batistoni P *et al* 2018 14 MeV calibration of JET neutron detectors-phase 2: in-vessel calibration *Nucl. Fusion* **58** 106016

[103] Litaudon X *et al* 2024 EUROfusion contributions to ITER nuclear operation *Nucl. Fusion* **64** 112006

[104] De Pietri M *et al* 2021 Integral modelling of the ITER cooling water systems radiation source for applications outside of the bio-shield *Fusion Eng. Des.* **171** 112575

[105] Radulović V *et al* 2021 Preparation of a water activation experiment at JET to support ITER *Fusion Eng. Des.* **169** 112410

[106] Villari R *et al* 2022 Neutronics, nuclear waste and safety activities within EUROfusion in support of preparation of ITER operations *32nd Symp. on Fusion Technology (SOFT2022)* (*Dubrovnik, Croatia*)

[107] Autran J L *et al* 2022 Real-time characterization of neutron-induced SEUs in fusion experiments at WEST tokamak during D-D plasma operation *IEEE Trans. Nucl. Sci.* **69** 501–11

[108] Dentan M *et al* 2024 Real-Time SER measurements of CMOS Bulk 40 nm and 65 nm SRAMs combined with neutron spectrometry at the JET Tokamak during D-D and D-T plasma operation *NSREC 2024 - 2024 IEEE Nuclear and Space Radiation Effects Conf.* (*Ottawa, Canada*)

[109] Mantsinen M J *et al* 2023 Experiments in high-performance JET plasmas in preparation of second harmonic ICRF heating of tritium in ITER *Nucl. Fusion* **63** 112015

[110] Kirov K K *et al* 2023 Impact of interaction between RF waves and fast NBI ions on the fusion performance in JET DTE2 campaign *Nucl. Fusion* **64** 016026

[111] Mantsinen M J *et al* 2024 Experiments with second harmonic ICRF heating of T in JET third major campaign with D-T plasmas (DTE3) *50th EPS Conf. on Plasma Physics* (*Salamanca, Spain*)

[112] Kazakov Ye O *et al* 2017 Efficient generation of energetic ions in multi-ion plasmas by radio-frequency heating *Nat. Phys.* **13** 973–8

[113] Kazakov Ye O *et al* 2023 Progress with applications of three-ion ICRF scenarios for fusion research: a review *AIP Conf. Proc.* **2984** 020001

[114] Kazakov Ye O *et al* 2024 Optimizing ion heating in D-T plasmas with three-ion ICRF scenarios: insights from JET and strategies for future tokamaks *50th EPS Conf. on Plasma Physics* (*Salamanca, Spain*)

[115] Schneider M *et al* 2021 Simulation of heating and current drive sources for scenarios of the iter research plan *Nucl. Fusion* **61** 126058

[116] Lerche E *et al* 2020 ICRH options for JET-ILW DTE2 operation *AIP Conf. Proc.* **2254** 030007

[117] Lerche E *et al* 2023 Fundamental ICRF heating of deuterium ions in JET-DTE2 *AIP Conf. Proc.* **2984** 030005

[118] Lerche E *et al* 2025 Heating D ions to optimal D-T fusion energies with ICRF waves (in preparation)

[119] Kirov K K *et al* 2024 Analysis of fusion alphas interaction with RF waves in D-T plasma at JET *Nucl. Fusion* **64** 086011

[120] Solano E R *et al* 2023 L-H transition studies in tritium and deuterium-tritium campaigns at JET with Be wall and W divertor *Nucl. Fusion* **63** 112011

[121] Piron L *et al* 2024 Psep/PLH control in Deuterium and Deuterium-Tritium JET plasmas *Plasma Phys. Control. Fusion* (https://doi.org/10.1088/1361-6587/adc8d0)
[122] Zotta V K *et al* 2024 Predictive modelling of JET baseline scenarios from DTE2 towards DTE3 *50th EPS Conf. on Plasma Physics* (*Salamanca, Spain*)
[123] Maslov M *et al* 2018 Observation of enhanced ion particle transport in mixed H/D isotope plasmas on JET *Nucl. Fusion* **58** 076022
[124] Bourdelle C *et al* 2018 Fast H isotope and impurity mixing in ion-temperature-gradient turbulence *Nucl. Fusion* **58** 076028
[125] Pitts R A *et al* 2025 Plasma-wall interaction impact of the ITER re-baseline *Nucl. Mater. Energy* **42** 101854
[126] Lennholm M *et al* 2024 Burn relevant D-T mixture control at JET *33rd Symp. on Fusion Technology (SOFT2024)* (*Dublin, Ireland*)
[127] Lennholm M *et al* 2024 Fusion Burn Regulation via Tritium Mixture Control in JET *Phys. Rev. X* submitted
[128] Piron L *et al* 2019 The dud detector: an empirically-based real-time algorithm to save neutron and T budgets during JET DT operation *Fusion Eng. Des.* **146** 1364–8
[129] Piron L *et al* 2024 Innovative dud detection based on JET DT experience *Fusion Eng. Des.* **200** 114155